12-2013

Standardized Longitudinal Connection Detail for Decked Precast Prestressed Concrete Girders

Ramzi Muftah Ali Abduallah
Western Michigan University

STANDARDIZED LONGITUDINAL CONNECTION DETAIL FOR DECKED PRECAST PRESTRESSED CONCRETE GIRDERS

by

Ramzi Muftah Ali Abduallah

A thesis submitted to the Graduate College
in partial fulfillment of the requirements
for the degree of Master of Science in Engineering (Civil)
Department of Civil and Construction Engineering
Western Michigan University
December 2013

Thesis Committee:

Upul Attanayake, Ph.D., Chair
Haluk Aktan, Ph.D.
Yufeng Hu, Ph.D.

STANDARDIZED LONGITUDINAL CONNECTION DETAIL FOR DECKED PRECAST PRESTRESSED CONCRETE GIRDERS

Ramzi Muftah Ali Abduallah, M.S.E

Western Michigan University, 2013

The use of decked precast prestressed concrete girders (DPPCG) is becoming popular in accelerated bridge construction. DPPCGs are assembled and connected on site using grout or concrete longitudinal connections. The durability performance of these connections is a concern. The objective of this research is to document the longitudinal connection behavior with respect to its design parameters, and establish a process for developing a standardized connection detail considering the demands due to live load and temperature gradient (TG) load. In order to demonstrate this process, decked bulb-tee and decked box-beam girders were considered. Finite element models, under various types and levels of loads and in conjunction with the design parameters, were used for evaluating the internal forces at connections. Structural analysis reveals that the TG load is significant and needs to be considered in connection design, and moment at connections increases when: (1) slab thickness increases, (2) bridge materials have greater strength and thermal properties, and (3) diaphragms have larger sections and smaller spacing. Structural design shows that (1) due to the TG moment, crack control criteria at service limit state governs the flexural design, and (2) tensile stress in steel in AASHTO (2012) eq. 5.7.3.4-1 should have an upper limit to prevent steel from yielding.

ACKNOWLEDGMENTS

First of all, I would like to thank Allah for giving me enough strength, power, and patience to complete this research. I would like to express my gratitude to my supervisor, Dr. Upul Attanayake, whose expertise, and understanding, supported my graduate experience. I appreciate his vast knowledge and skills. Very special thanks go out to Dr. Haluk Aktan, without his continuous advising I would not complete my research as it should be. I also thank Dr. Yufeng Hu for being a member in my committee.

Sincere thanks go out to my family especially my mom whose love guides my success. Also, I acknowledge my friends, colleagues, who supported me to finish my thesis. Lastly, I thank the Libyan society who financed me to enhance my education.

Ramzi Muftah Ali Abduallah

TABLE OF CONTENTS

Table of Contents-Continued

Table of Contents-Continued

Table of Contents-Continued

APPENDICES

LIST OF TABLES

LIST OF FIGURES

List of Figures-Continued

List of Figures-Continued

CHAPTER 1

INTRODUCTION

1.1 OVERVIEW

Accelerating bridge construction (ABC) is getting acceptance by Departments of Transportation (DOTs) to minimize traffic disruption and ensure safety for the public and construction workers. The elimination of formwork use and improvement of work-zone safety are items that have a greater impact on the choice of bridge system type. The economic impact associated with the closure of high traffic volume roads with long detours is taken into consideration when selecting ABC alternatives. When all these factors are combined, prefabricated bridge elements and systems is one of the preferred choices. In particular, decked steel girders and decked precast prestressed concrete girders (DPPCGs) are a highly desired option for accelerating bridge construction. Decked bulb-tee (DBT) and decked box-beam (DBB) are two examples of DPPCGs.

DPPCG consists of an integral deck that is cast and prestressed at the same time as the girder. Prefabricated bridge elements are manufactured under controlled conditions in the precast plant, which assures high quality units. That is, superstructure components work efficiently against induced stresses, enhancing the durability of the deck and consequently minimizing the life-time cost of the bridge. The use of DPPCG is beneficial in regions that have shorter construction seasons, very high traffic volumes, and long detours. Since DPPCG encompasses the bridge deck slab, the time needed to erect formwork and allow concrete to cure at the construction site is minimized.

Superstructure elements are transported, assembled, and connected at a construction site with cast-in-place joints. The load transfer between the adjacent PPCGs relies on the strength of the connections. Further, the durability performance of these systems heavily depends on the field-cast connections. Different connection types are used for joining girder flanges (e.g., shear and shear-flexure transfer connections).

Despite the benefits that DPPCG offers, it is still used in only a handful of states. Concern about the lack of connection design specifications is the main barrier to the widespread use of this superstructure system (Ma et al. 2007).

1.2 PROBLEM STATEMENT

Culmo (2009) and French et al. (2011) provide details for deck level connections. Even though the majority of connections with these details perform satisfactorily in terms of strength, challenges with ensuring durability have been documented (Stanton and Mattock 1986; Ma et al. 2007; Oesterle and Elremaily 2009). Since the ABC is becoming more popular among state DOTs, there is a current emphasis on developing a standardized connection detail. Unfortunately, there is not a comprehensive document detailing the standardized connection detail development process. The studies so far have investigated load capacity of the connections under static and dynamic loads. Even though the American Association of State Highway and Transportation Officials (AASHTO) (2012) emphasizes the need for incorporating temperature gradient (TG), none of the previous studies have investigated the impact of TG on connection behavior and load demand.

1.3 OBJECTIVE

The primary objective of this research is to present a comprehensive process for developing a standardized detail for durable deck level longitudinal connections. Particularly, the objectives are to: (1) develop a process for standardizing longitudinal connection detail, (2) calculate load demand (i.e., moment, shear, and axial force) due to live load (LL) and TG at the connection, and (3) provide a standardized detail for deck level longitudinal connections. A detailed example is presented to demonstrate the development of the design detail incorporating LL and TG.

1.4 SCOPE

The study will illustrate the process of developing standardized connection details for deck level longitudinal connections between PPCGs. Decked bulb-tee and decked box-beam girders were chosen to illustrate the process. The applicable loads are selected from AASHTO (2012) as LL and TG. Since the standardized connections are intended to be implemented in Michigan, AASHTO (2012), Michigan Department of Transportation (MDOT) Bridge Design Manual (MDOT 2013a), and MDOT Bridge Design Guide (MDOT 2013b) stipulations are adhered to.

CHAPTER 2

RESEARCH METHODOLOGY

The process of standardizing connection detail is depicted in Figure 1. Connection types, loads, and design parameters are identified through a comprehensive review of the literature with respect to state-of-the-art connection detail practices identifies connection types, loads, and design parameters. Hence, the following three major topics are the focus of the literature review:

- Longitudinal connection types, details, and performance
- The applicable loads
- Design parameters that are expected to have an influence on the longitudinal connection load demand

Structural analysis of bridge models evaluated the significance of the design parameter effects on connection load demand, identifying critical design parameters. Based on these parameters, the structural analysis of a final bridge model identified the greatest possible connection load demand as a result of TG and LL. The ultimate product of this research is a standardized connection detail that satisfies these load demands. An improved durability performance and strength equal to that of the rest of the prefabricated modules of the bridge are expected from the standardized connection detail.

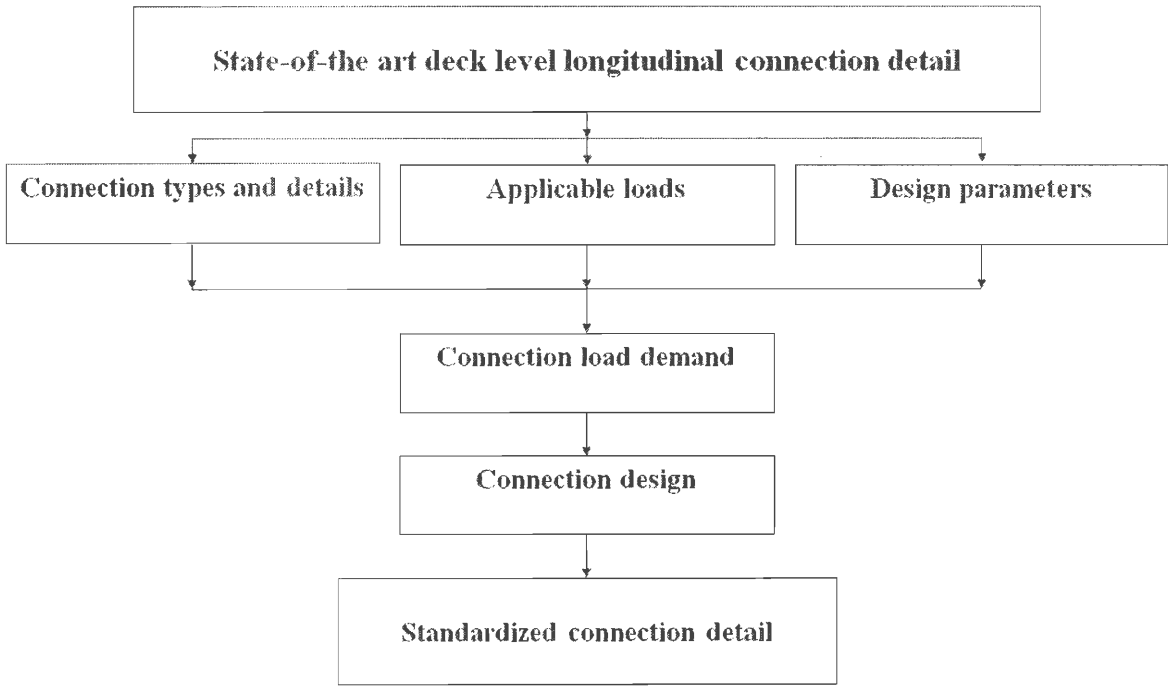

Figure 1. Research Methodology

CHAPTER 3

LITERATURE REVIEW

3.1 OVERVIEW

This chapter presents (1) superstructure component configurations, (2) longitudinal connection types, details, and performance, (3) bridge geometry, (4) diaphragm configurations and spacing, (5) materials, and (6) load types and magnitude.

3.2 SUPERSTRUCTURE COMPONENT CONFIGURATIONS

Two systems of DPPCGs, DBT and DBB, were selected for the study as a result of the advantages they offer to ABC. Several DOTs and construction agencies have developed DBT standard sections with different details and span capabilities. On the other hand, the standard DBB has not yet been developed. Due to their widespread use, Precast/Prestressed Concrete Institute (PCI) standard sections were selected for this study.

3.2.1 Decked Bulb-Tee Girder (DBT)

A DBT is made up of either a prestressed concrete I-beam or bulb-tee girder that is simultaneously cast with an integral deck. Figure 9 shows the geometry of PCI (2011) DBT standard sections, which are typically manufactured with 4 ft, 6 ft, and 8 ft wide flanges. As the use of wider sections is more economical (SHRP2 2012), the analytical study investigated 6 ft and 8 ft wide girders. Figure 3 summarizes the maximum applicable span for each DBT girder size. DBTs of different sizes are named using their section total depths. For instance, "DBT-35" refers to a decked bulb-tee girder with a total depth of 35 inches.

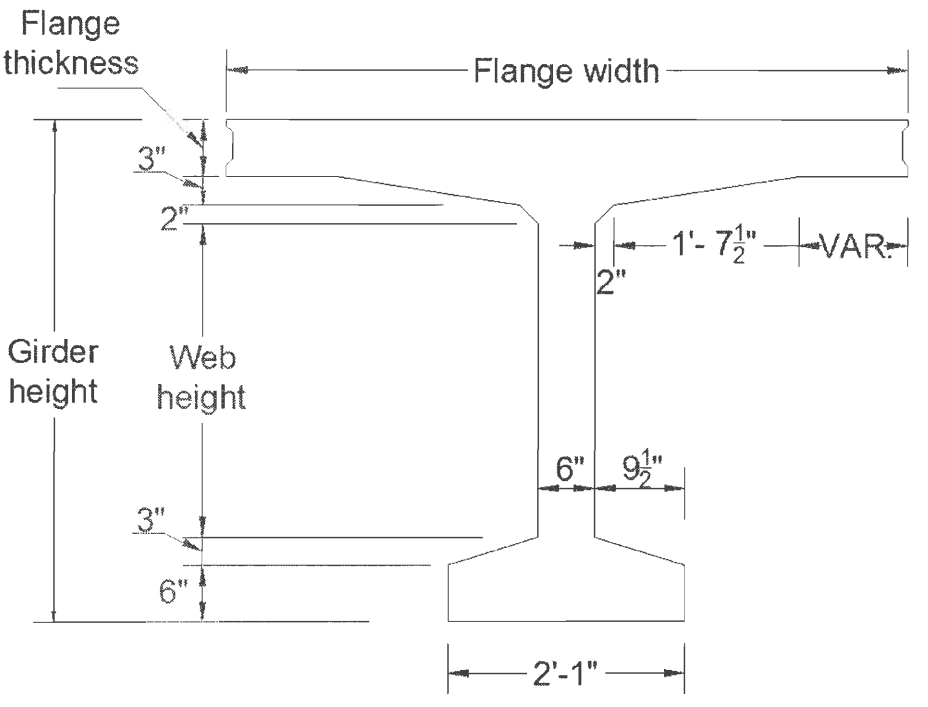

Figure 2. Standard PCI DBT

Use of the maximum applicable span for a certain prefabricated girder size is limited by the capability of trucks and cranes. For instance, MDOT (2013a) limits the weight of a prefabricated module to 80 kips. However, a typical crane lifting capacity is up to 200 kips (SHRP2 2012). Therefore, Figure 4 shows the maximum girder span length capacity that can be constructed without exceeding weight restrictions (i.e., 80 kips and 200 kips). For example, the maximum span capacity of DBT-65 is 170 ft, but if the full span capacity of this girder is utilized, the weight will exceed the weight limit. Therefore, not more than 159 ft of DBT-65 can be constructed if the maximum weight limit is 200 kips, and not more than 63.5 ft if the maximum weight limit is 80 kips.

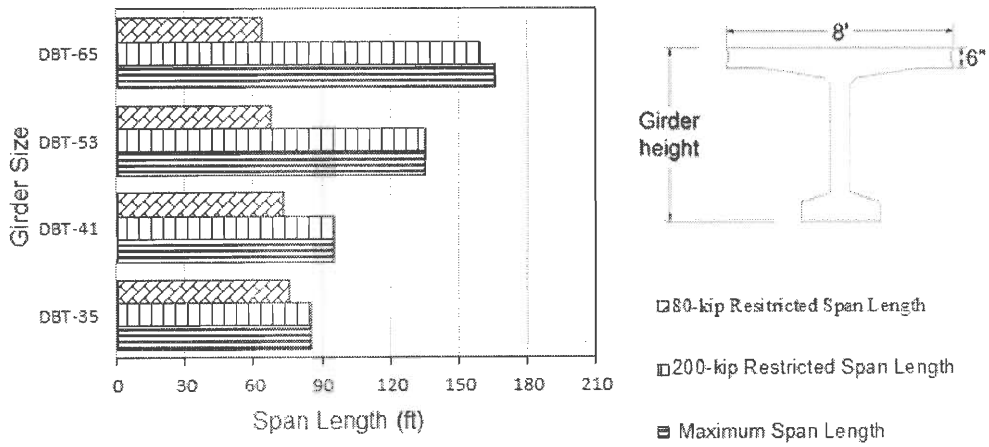

Figure 3. Maximum Applicable and Weight Restricted Span Lengths of DBT with 6 in. Thick Flange

However, if the construction of a U-bar connection is intended, a 6 in. thick flange is not sufficient to accommodate both concrete cover and the bend diameter of the bar, as specified in AASHTO (2012). MDOT (2013b) stipulates that the standard deck slab thickness is 9 in. Typically, a 0.5 in. sacrificial layer is added to the girder flange thickness for grinding purposes (e.g., camber adjustment). Thus regardless of the changes in prestressed concrete design due to the extra size and weight of the girder, the weight restricted span lengths from Figure 3 are reduced as a result of the extra weight added by the increase in flange thickness from 6 in. to 9.5 in. (Figure 4).

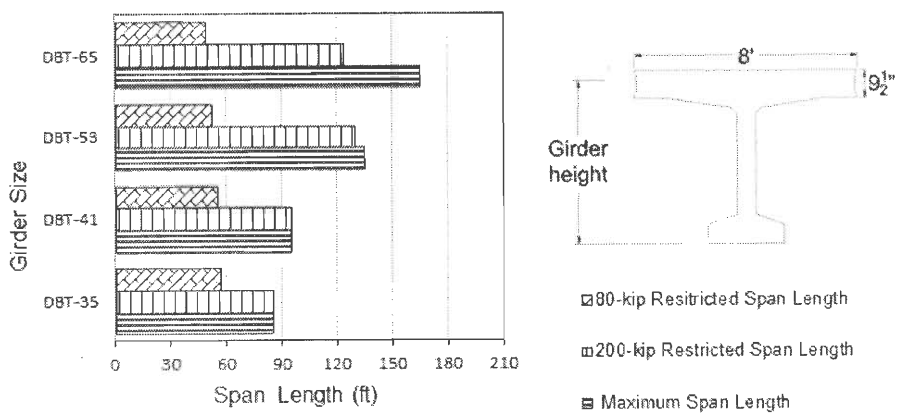

Figure 4. Maximum Applicable and Weight Restricted Span Lengths of DBT with 9.5 in. Thick Flange

Figure 6. Maximum Applicable and Weight Restricted Span Lengths of DBB with 9.5 in. Thick Flange

3.3 LONGITUDINAL CONNECTION DETAIL

Different details of deck level connections are used in practice. Comprehensive reports, such as Connection Details for Prefabricated Bridge Elements and Systems (Culmo 2009), provide most of the connection details that are either standard practice or experimental/conceptual. It should be noted here that since DBTs are considered one of the most promising DPPCGs, the longitudinal connection details between these members have been extensively studied. AASHTO (2012) specifies two types of connections between prefabricated units based on load transfer mechanism: shear and shear-flexure transfer connections.

3.3.1 Shear Transfer Connection

According to Martin and Osborn (1983), Stanton and Mattock (1986), and Oesterle and Elremaily (2009), DBTs are commonly connected by a combination of welded transverse tie connections with keyways filled with either non-shrink cementitious grout or a custom-designed concrete mix (Figure 7). A 6 in. thick flange is adequate to develop

3.2.2 Decked Box-Beam (DBB)

A DBB is made up of a prestressed concrete box beam that is simultaneously cast with an integral deck. The standard DBB has not yet been developed. However, Texas DOT has devised a similar bridge superstructure system called a decked slab beam (TXDOT 2013). This type of DPPCG is included here since most of the aging bridges in the USA have obsolete vertical clearances (Svirsky 2013). Therefore, the use of shallow DPPCGs is a practical option for a bridge superstructure replacement. Furthermore, the applicable span of DBBs is appropriate for short-to-medium span lengths, which is the focus of this research (Reference). However, since no standard sections of DBBs are available, PCI (2011) box beams were chosen and hypothetically considered as decked box-beams for study consistency. Consequently, span applicability ranges for different sizes of DBB girders were assumed to be the same as those for box beams. In this research, DBB is named by the box beam depth and width. For instance, "DBB-I-36" refers to a decked box-beam that is 27 in. deep and 36 in. wide. Figure 6 shows the maximum applicable and weight restricted span lengths for each girder size. The maximum applicable span lengths for DBBs were assumed to be the same as those for box beams. It should be noted that Figure 6 shows three bars with the lowest bar showing the maximum applicable span lengths and the upper two bars showing the span lengths when weight restrictions of 200 kips and 80 kips are considered.

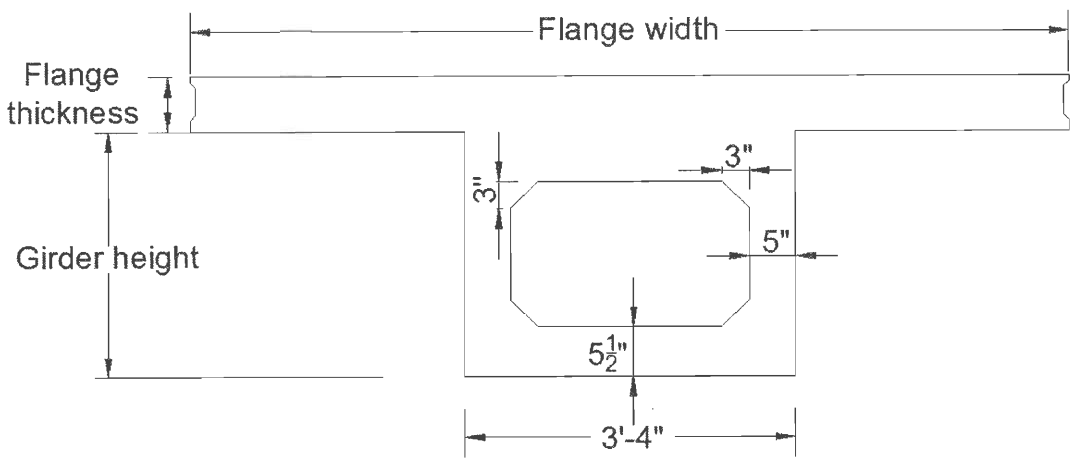

Figure 5. Standard PCI Box Beam Converted to DBB

a shear transfer connection. This detail is designed merely to transfer shear between neighboring girders (Culmo, 2009). The welded transverse ties work as mechanical connections. Typically, they are plates anchored into girder flanges with shear studs or deformed bar anchors.

The intervals between the ties range from 4 ft to 8 ft in order to ensure enough tensile capacity against movement in the transverse direction. However, DOTs and bridge construction agencies construct shear transfer connections with different details (Figure 8 and Figure 9). The main function of the shear key is providing primary wheel load transfer between adjacent girders (Martin and Osborn 1983). A shear transfer connection works as a hinge by transferring only vertical forces between the two neighboring girders (AASHTO 2012). Thus, each flange of the girder is designed to work as a cantilever (Culmo 2009). Yet, the overall rigidity of the connection may cause a small portion of the moment to be transferred between the girders (Martin and Osborn 1983; Stanton and Mattock 1986). Shear forces along the length of the connection are not distributed evenly (i.e., concentrated at the connectors). As a consequence, the connection section may not work efficiently, increasing the chance for cracks to develop at certain locations between the connectors (Ma et al. 2007).

A survey conducted by Oesterle and Elremaily (2009) indicated that grouted shear keys with welded transverse ties have good-to-excellent performance. However, durability of these connections is a concern. Since the welded connectors are spaced widely, cracks develop in the shear key and propagate through the overlay. These cracks allow moisture ingress through the connections. Spalling and delamination are results of corrosion due to moisture ingress (Ma et al. 2007). Stanton and Mattock (1986) stated that moment at connections is the major cause of these cracks. Bridge designers have raised concerns about the long term fatigue behavior of welded tie connections, especially on roads with heavy average daily truck traffic. Other defects that might be found on shear transfer connections with welded ties and shear keys are: (1) the bottom surface of the welded plate may corrode if it is not stainless steel, leading to connection

failure and (2) when the grout is not well-filled, the mechanical interlock is not adequate or completely nonfunctional (Martin and Osborn 1983; Li 2009).

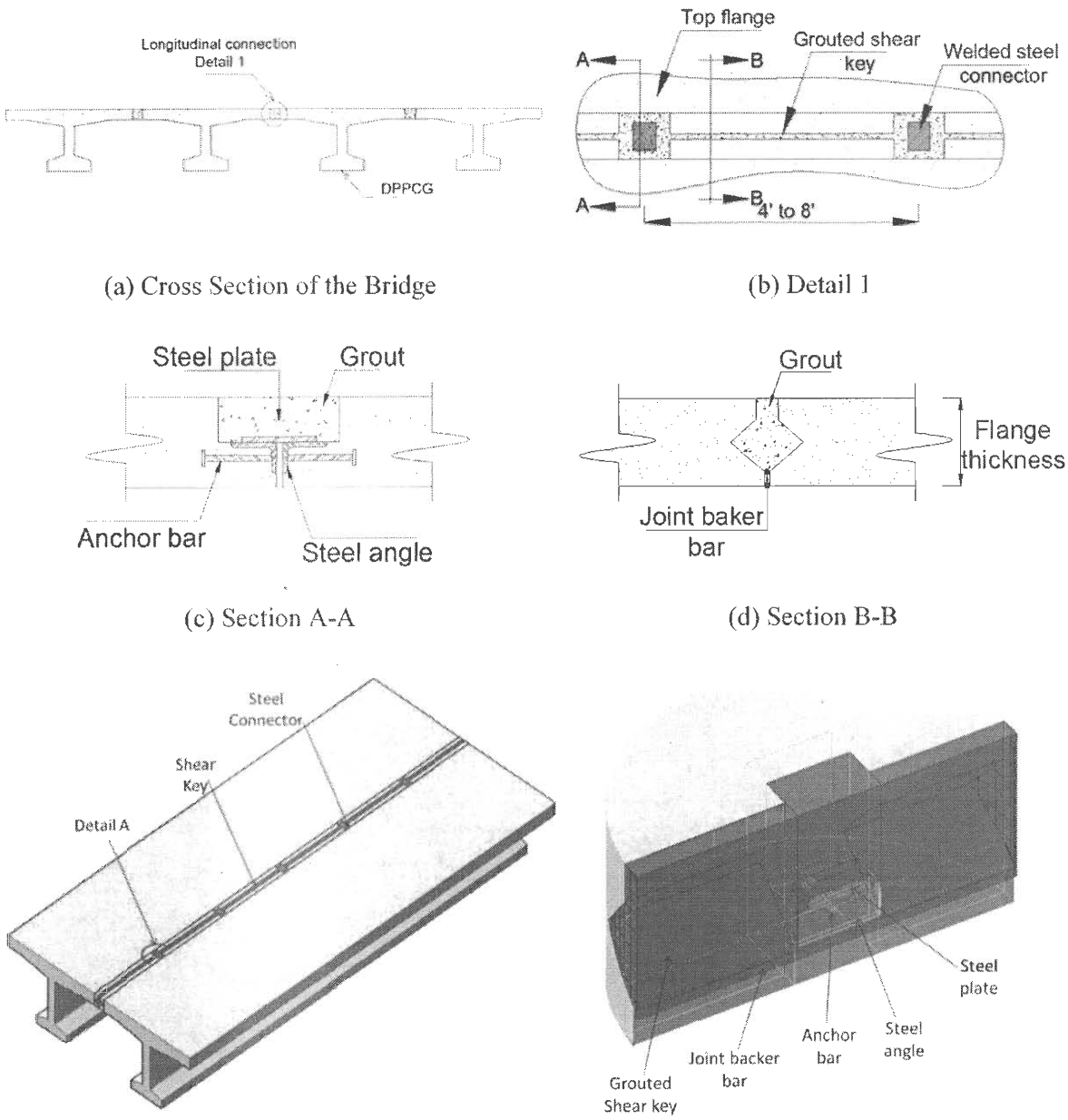

(a) Cross Section of the Bridge

(b) Detail 1

(c) Section A-A

(d) Section B-B

(e) 3D Configuration

(f) Detail A

Figure 7. DBT Girders Connected by Longitudinal Joints with Welded Steel Connectors (Source: Stanton and Mattock 1986)

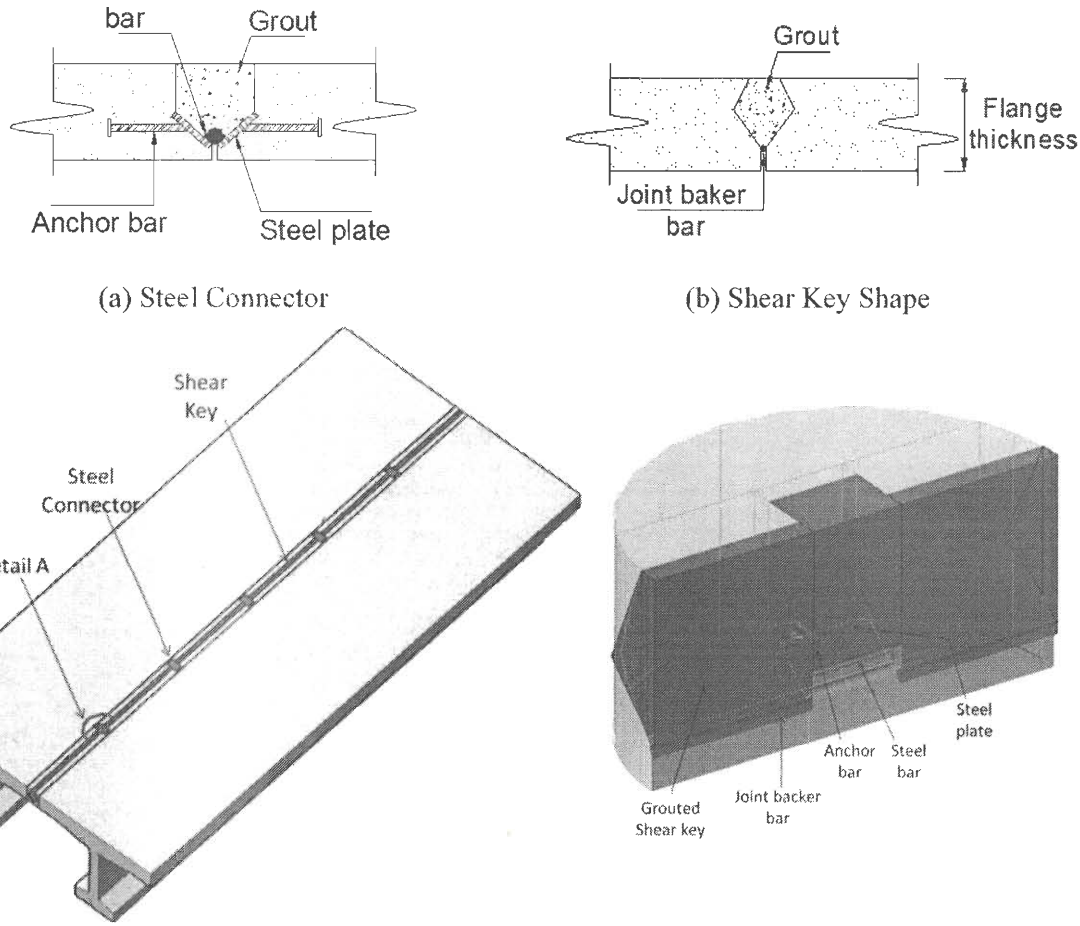

(a) Steel Connector

(b) Shear Key Shape

(c) 3D Configuration

(d) Detail A

Figure 8. Common Shear Transfer Connection Detail 1 (Source: Oesterle and Elremaily 2009)

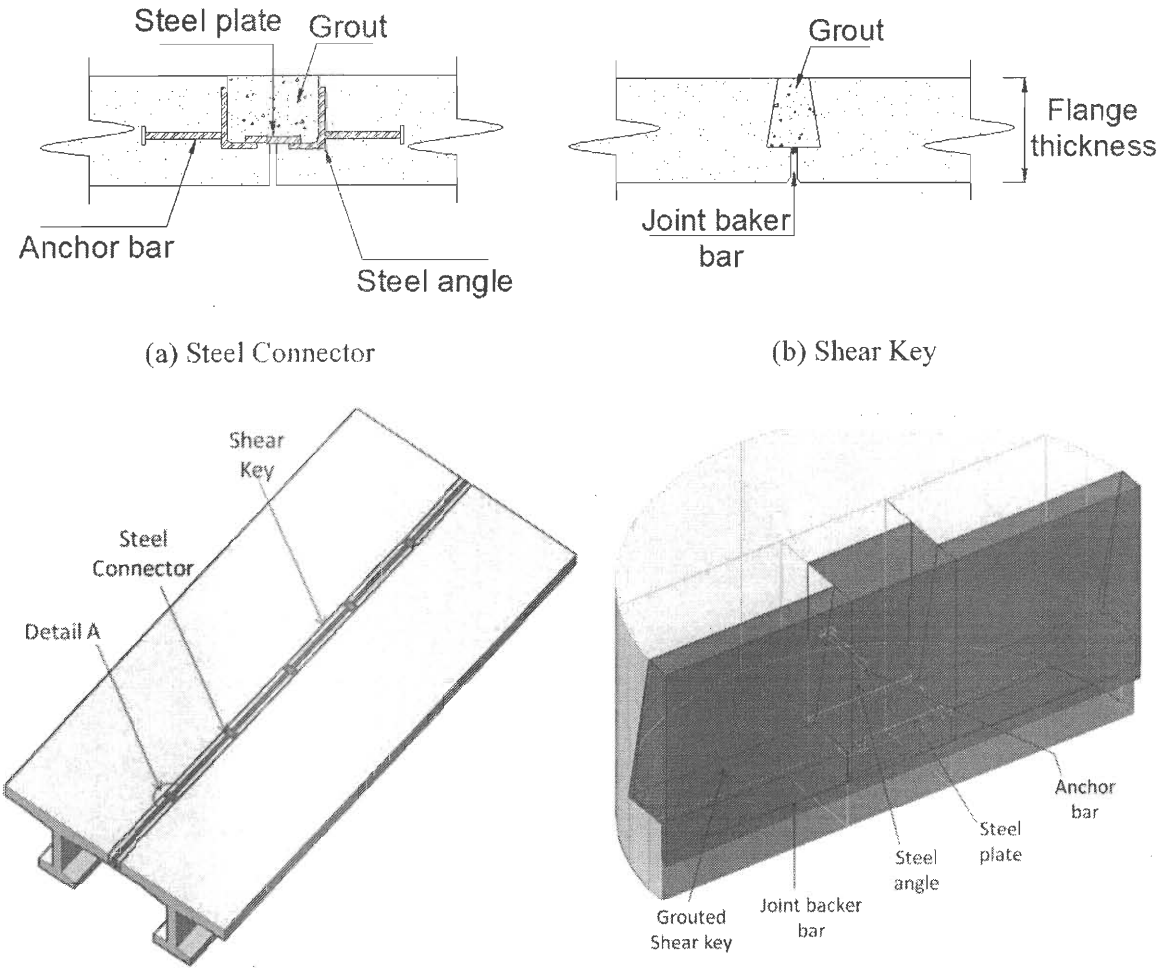

(a) Steel Connector

(b) Shear Key

(c) 3D Configuration

(d) Detail A

Figure 9. Common Shear Transfer Connection Detail 2 (Source: Oesterle and Elremaily 2009)

3.3.2 Shear-Flexure Transfer Connection

The other way to connect DPPCGs is to use connections that are capable of transferring shear and moment between neighboring girders. This can be achieved by reinforcing the connection with bars. Bars project from the girder flanges and overlap into the joint. Lacer bars along the connection length are provided to enhance the mechanism of the connection. This type of connection is intended to provide full

continuity between prefabricated superstructure modules and control the potential crack width (AASHTO 2012).

Crack widths at connection locations can be controlled more efficiently through the use of well-distributed reinforcement bars (AASHTO 2012). That is, both material bonding strength and connection reinforcement bars resist the induced stresses. A shear-flexural transfer connection has several reinforcement details that are in practice (e.g., straight bars, headed bars, and U-bars). Connections with straight bars require the use of a high bonding material (e.g., ultra-high performance concrete). With conventional concrete, U-bars and headed bars are commonly used to minimize the width of connection, since they are stronger and require less development length (French et al. 2011).

3.3.2.1 U-bar detail

U-bars are formed from single bars bended to provide two layers of reinforcement (Figure 10). Projecting bars from adjacent flanges lap into the connection to provide continuity for deck reinforcement. The typical reinforcement bar sizes used in longitudinal connections are #4 and #5 bars. The development length is minimized by the 180° bend of the U-bar that forms a mechanical anchorage (Jorgensen and Hoang 2013). In accordance with AASHTO (2012), the bend diameter shall not be less than $6d_b$, where, d_b is the bar diameter. If MDOT (2013b) requirements for concrete cover are imposed, a 6 in. thick flange is not sufficient. Thus, an increase in girder flange thickness is needed. However, this results in an increase in the precast module weight. Precast element weight and space issues need to be considered during constructability evaluation (Attanayake et al. 2012). The interface of the abutted flanges is detailed to be female-to-female shear key, increasing the bonding face area and enhancing the connection resistance against shearing forces. Narrow connection widths are preferred in order to minimize filling material costs. Furthermore, reducing the width also shortens curing time of the filling material at the construction site (SHRP2 2012). The strength of the U-bar connection is

maintained by the bearing surface of the U-bar (i.e. the inside of the bend). Additionally, lacers are provided to enhance the mechanism of the looped bars (He et al. 2013).

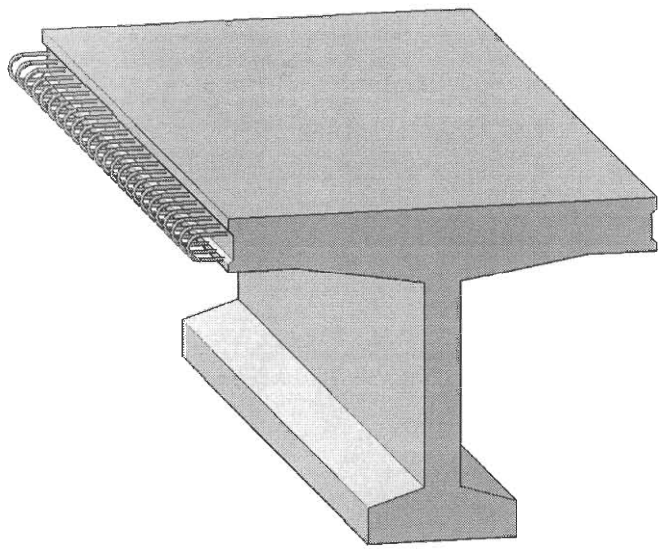

Figure 10. U-Bar Detail for DBT

Even though the use of U-bars provides good crack width control and enhances connection durability, the lack of standard specifications for deck level connections concerns ABC users. The behavior and strength capacity of the connections with different reinforcement details and widths have been evaluated. Tensile and flexural capacity results were monitored to check the connection strength against cracking. French et al. (2011) performed a laboratory test on a U-bar detail and a headed bar detail connections. The test results indicated that a U-bar joint with a 6 in. overlap length and two longitudinal lacer bars produces the largest flexural and tensile capacity with an adequate ductility. In addition, the researchers concluded that at the service level, cracks are relatively small in the case of constructing a U-bar connection detail. From a practical point of view, a phone survey indicated that DOTs and bridge construction agencies prefer U-bars over other reinforcement details for deck level longitudinal connections. As well, the U-bar detail is preferred in Japan and Korea (French et al 2011).

3.3.2.2 Headed bar detail

A headed bar detail consists of one row of bars protruding from the middle of the flange thickness and overlapping into the connection (Figure 11). The bars are placed at the mid-thickness of the flange due to concrete cover satisfaction (He 2013). The bearing surface (i.e. the head) provides strength to the connection (Li 2009). The abutted flanges are made to be female-to-female shear key and mostly V-shaped in order to optimize the connection shear resistance. Analytical and experimental studies have been carried out to evaluate the performance of the headed bar detail. Oesterle and Elremaily (2009) concluded in their study that the headed bar detail has enough strength capacity to transfer full moment and shear between adjacent girders. Since there is no need to increase deck flange thickness, headed bar detail is considered as a viable longitudinal connection detail and it might be a substitute to the combination of the welded tie connectors with grouted shear key (Li 2009).

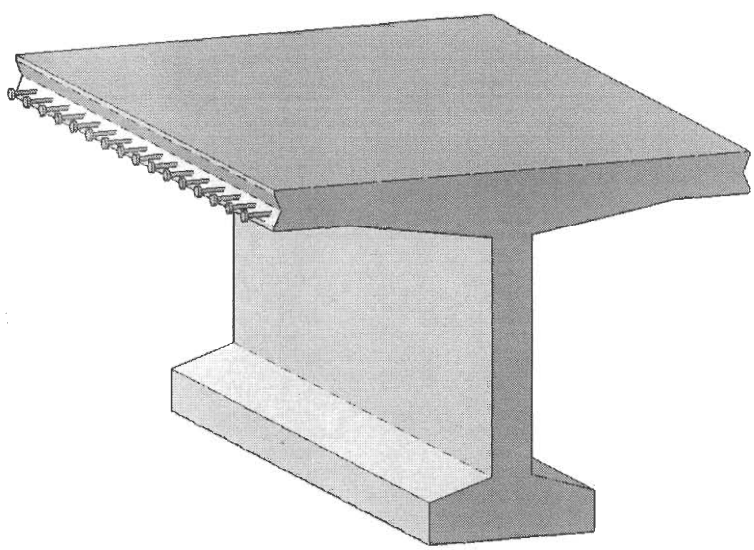

Figure 11. Headed Bar Detail for DBT

However, when a bridge is in service, peak stresses develop at the extreme surfaces of the connection (i.e., top and bottom surfaces). Therefore, the use of a headed bar layer located at the mid-thickness of the flange is not optimal for crack control. Other

experimental studies evaluated the use of two layers of headed bars. Due to the large diameter of heads, the concrete cover requirement is not fulfilled (Li 2009).

3.3.2.3 Ultra-High Performance Concrete Connections

Durability and constructionability issues necessitate the use of innovative materials for bridge construction (e.g. Ultra-High Performance Concrete (UHPC)). An optimized mixture of cement, water, and aggregate compose UHPC. A low cement to water ratio and a high percentage of discrete fiber reinforcement produce UHPC with compressive strength and modulus of elasticity exceeding 18 ksi and 6200 ksi, respectively (Graybeal 2012). UHPC connections are female-to-female (diamond shaped) shear key, reinforced with straight or headed lapped bars (Russell and Graybeal 2013) (Figure 12 a, and b).

According to laboratory tests performed by Graybeal (2012) and Hartwell (2011), when deck-level connections are built with UHPC: (1) the structural behavior of connections emulates a cast in place concrete bridge deck, (2) connections that are 6 in. wide and 6 in. thick can develop sufficient development length and flexural and tensile capacity, (3) connections with straight bars are able to provide sufficient strength to transfer shear and moment between adjacent girders, and (4) the bonding capability is higher, mitigating the occurrence of interface debonding. In contrast, SHRP2 (2012) conducted an intensive laboratory test on UHPC connections and revealed that even though the UHPC deck connections manifest high strength, interface debonding occurred. Tensile testing clarified this, with debonding occurring as a result of forces much lower than the forces imposed when the bridge is in service. In addition, Shim (2005) addresses durability concerns regarding early-age cracking that might develop during the manufacture of UHPC components. This study indicates that the high percentage of cement in UHPC increases the temperature during hydration, initiating micro-cracks that allow chemicals to penetrate and cause deterioration.

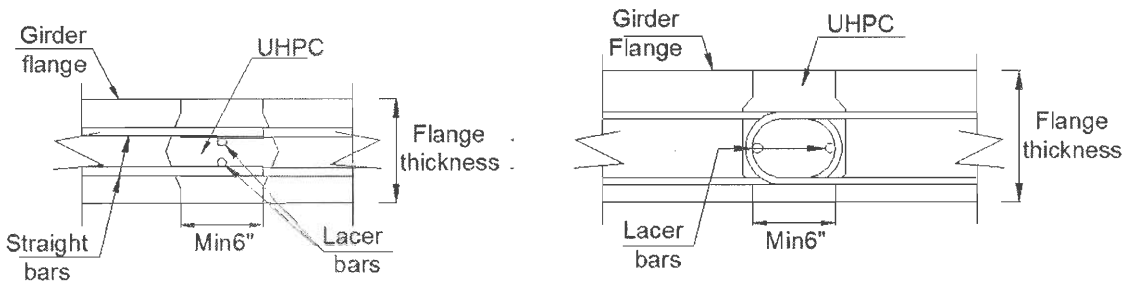

(a) Straight Bar Detail (b) U-Bar Detail

Figure 12. UHPC Longitudinal Connection Detail

UHPC connections were tested in the field during the US Highway 6 Bridge over Keg Creek project in Iowa. The ultimate goal of this project was to evaluate the performance of the latest innovative materials and techniques in bridge construction. The Keg Creek Bridge is the first bridge in the USA that was built out of HPC prefabricated decked steel girders connected with UHPC joints. The longitudinal connections are 6 in. wide and 8 in. deep and reinforced with #5 hairpin bars at 8 in. spacing. The bridge was constructed in 2011. Seven months later, cracking was documented at the interface between UHPC connections and girder flanges (Figure 13) (Phares et al. 2013).

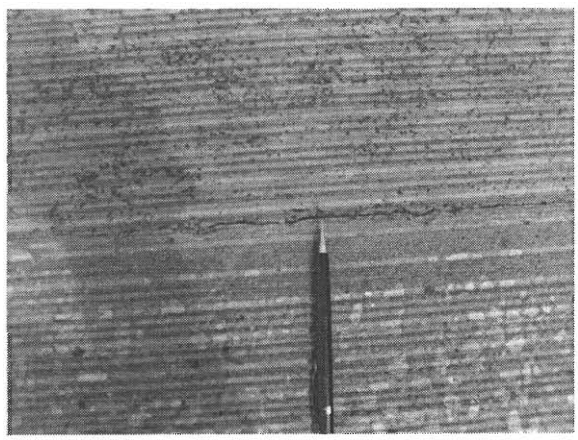

(a) Deck Top Surface Cracking

(b) Deck Bottom Surface Cracking

Figure 13. Cracking at the Interface of the UHPC Longitudinal Connection (Source: Phares et al. 2013)

3.3.2.4 Lacer Bars

Connections with distributed bars have to include lacer bars, since lacer bars have a major role against the premature failure of connections, such as local crushing and splitting (Dragosavi'c et al. 1975). Typically, two Lacers are placed along the length of the connection at the internal face of the looped (Figure 14) (French et al. 2011). The mechanical anchorage performs more efficiently when lacers are provided. However, the size of lacers has to be sufficient to be able to transfer forces from the bearing surfaces (i.e., the inside of the bend for the U-bar) to the concrete core (He et al. 2013). Gordon and May (2005) carried out laboratory testing on U-bar connections to evaluate the significance of the lacer bars. The specimen was a U-bar connection without lacers. The connection had an abrupt failure due to the lack of confinement that would be provided by the lacer bars.

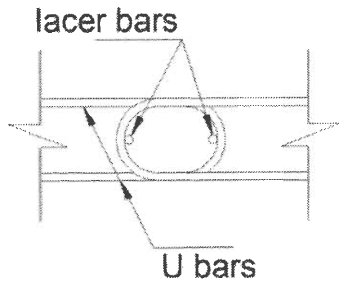

Figure 14. Lacer Bar Location

3.4 BRIDGE GEOMETRY

This study focused on routine bridges (i.e., bridges with a span ≤130 ft and skew ≤ 45^0), which represent the majority of Michigan bridges (Pontis 2010). SHRP2 (2012) emphasized the need for assigning weight and size limitations for prefabricated modules in the way that traditional transportation and erection equipment (e.g., trucks and cranes) can be utilized. Moreover, if the use of high capacity equipment is mandatory, the extra relative costs should be taken into consideration. Dimensional and weight restrictions for prefabricated modules have been adopted depending on typical equipment capacity by SHRP2 (2012) as listed below. These restrictions were selected based on the use of available transporting and lifting equipment without a significant increase in time and/or cost as a consequence of the use of unconventional devices.

- Length ≤130 ft,
- Weight≤ 100 tons (200 kips), and
- Width ≤ 8 ft

3.4.1 Bridge Span Length

More than 95% of the bridges in Michigan have span length less than or equal to 130 ft as indicated in Figure 15 (Pontis 2010). Considering the span ranges presented in the SHRP2 (2012), span length is grouped to:

- 40 ft ≤ Span ≤ 70 ft
- 70 ft < Span ≤ 100 ft
- 100 ft < Span ≤ 130 ft

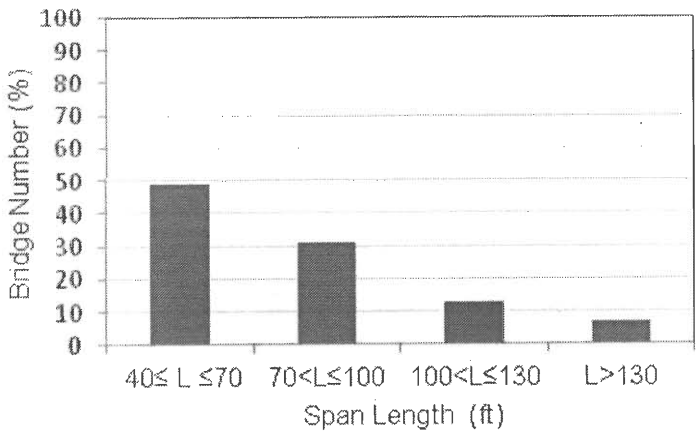

Figure 15. Length Ranges of Michigan Bridges (Source: Pontis 2010)

3.4.2 Skew

The most common ranges for skew are 20°, 30°, and 45°. The skew angle influences diaphragm distribution. DOTs have different skew policies. According to Pontis (2010), more that 90% of the bridges in Michigan have a skew ≤ 45° (Figure 16).

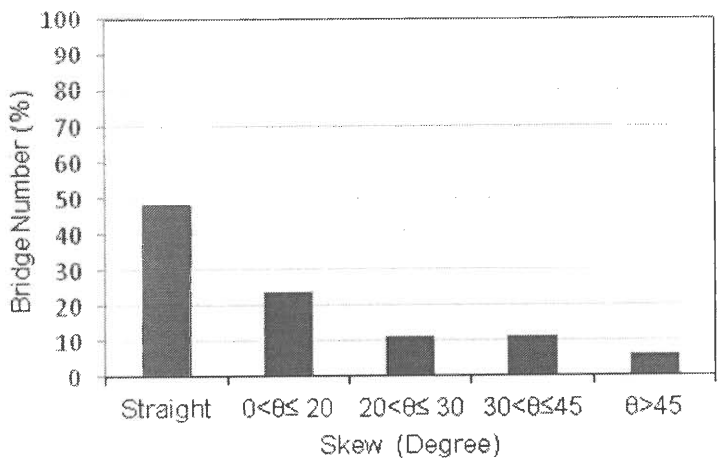

Figure 16. Skew Ranges of Michigan Bridges (Source: Pontis 2010)

3.5 DIAPHRAGM CONFIGURATION AND SPACING

Diaphragms are constructed from either concrete or steel. Diaphragms at abutments and piers are mandatory. Conversely, it is not obligatory to build intermediate diaphragms if the bridge designer does not see an importance for it through the structural analysis (AASHTO 2012). Every DOT has its own specifications for diaphragms. This section presents the diaphragm requirements that are commonly used.

3.5.1 End Diaphragm

End diaphragms work as ties at the end of girders. They hold the end of the girders and work simultaneously against loads on the bridge. The main function is to help transfer loads among girders and from the superstructure to the substructure (abutments and/or piers) (Oesterle and Elremaily 2009). Typically, end diaphragms are made of concrete that is either precast or cast in place. Some of them are integrated with the backwall (e.g., integral and semi-integral backwall). The total depth and width vary among precast manufacturers. Figure 17 shows diaphragm configurations with various depths for a DBT bridge system. For a DBB bridge system the end diaphragms are mostly full depth (Figure 18).

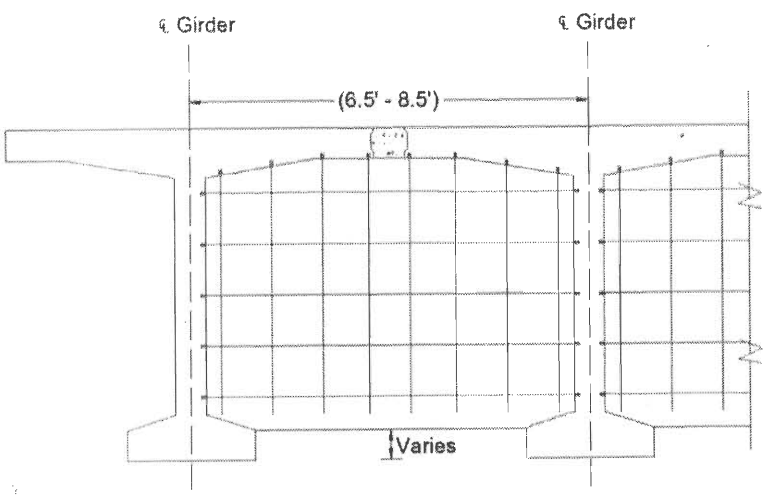

Figure 17. End Diaphragm Configuration for DBT

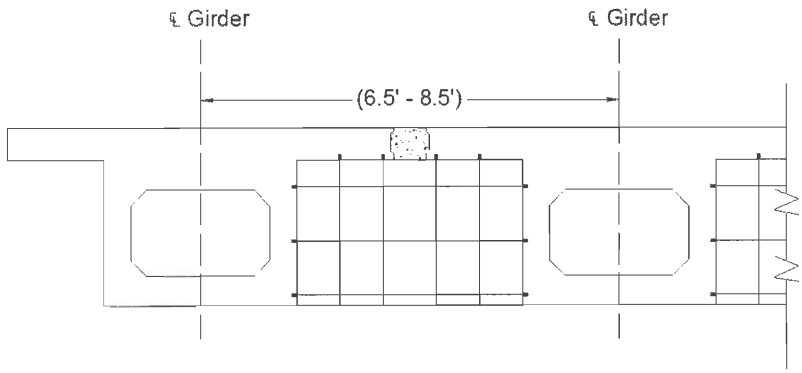

Figure 18. Full Depth End Diaphragm for DBB

3.5.2 Intermediate Diaphragms

Using intermediate diaphragms may slow construction. Therefore, ABC users usually try to choose an intermediate diaphragm system that helps minimize bridge assembly time (SHRP2 2012). This section presents the possible types of intermediate diaphragms that can be constructed for DBT and DBB. In particular, diaphragm size and spacing of intermediate diaphragms are presented.

3.5.2.1 DBT Intermediate Diaphragms

Intermediate diaphragms are made of either concrete or steel. Figure 19 shows intermediate concrete diaphragms used with DBT. Steel diaphragms require less on-site work and are lighter. Figure 20 shows a cross frame diaphragm and Figure 21 shows K-bracing. Both diaphragm configurations are used with DBT because of the simplicity of construction and the efficiency in transferring loads between girders (Culmo 2009; PCI 2011). The most common spacing requirements for intermediate diaphragms are:

- One or no diaphragm for span $\leq$ 80 ft,
- Two diaphragms at 1/3 points for 80 < span $\leq$ 120 ft, and
- Three diaphragms at 1/4 points for span > 120 ft.

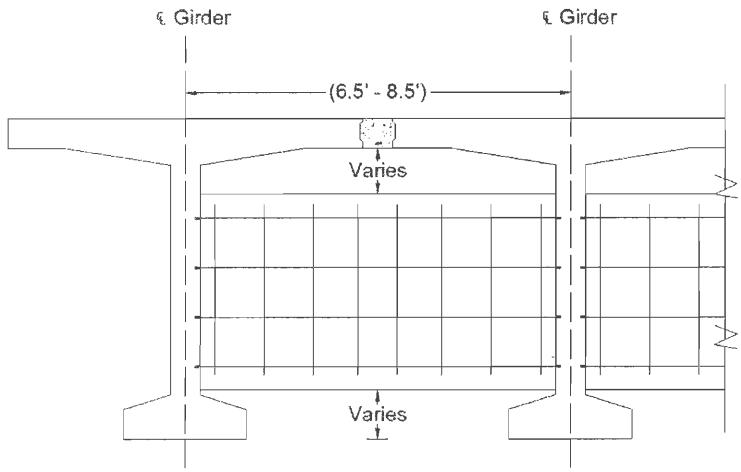

Figure 19. Intermediate Diaphragm Configuration for DBT

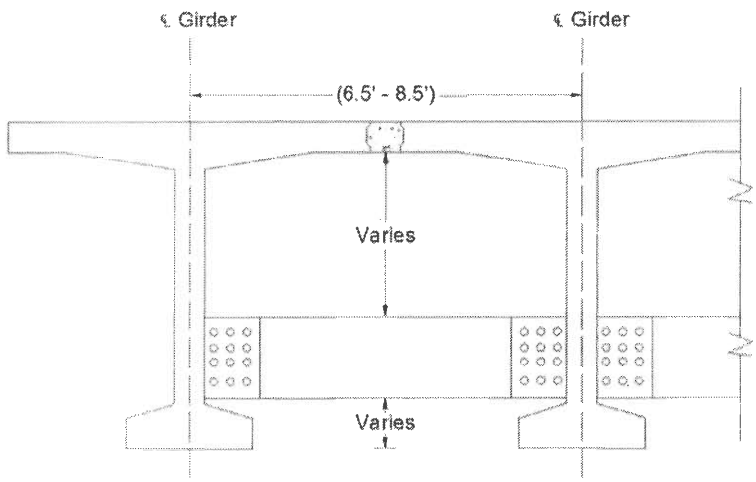

Figure 20. Steel Diaphragm (Cross Frame)

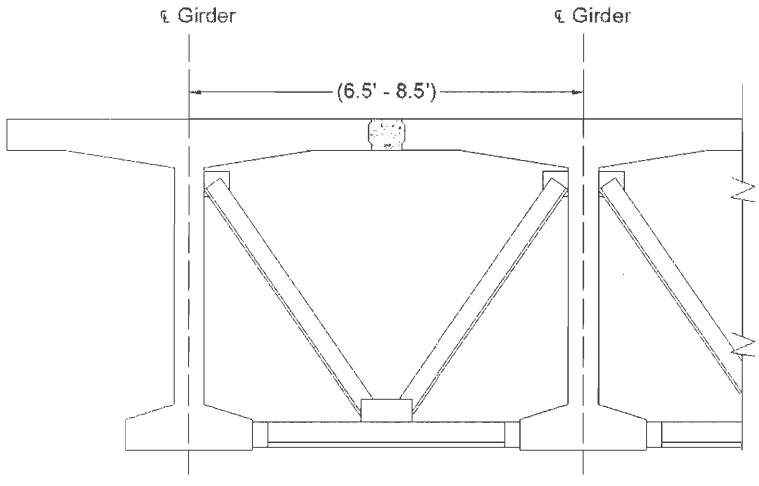

Figure 21. Steel Diaphragm (K-bracing)

3.5.2.2 DBB Intermediate Diaphragms

Generally, the same intermediate diaphragm requirement for box beams is used for DBB. Spacing and size of diaphragms are based on post-tensioning specifications (i.e., duct location and width) (MDOT 2013b). The geometry of the intermediate diaphragms is similar to the end diaphragms (Figure 18).

3.6 MATERIAL PROPERTIES

The main components of grout are: cement, sand, and water. Additives are mixed with these main components to improve the grout characteristic (e.g., easy flow, self-compacting, and expansive) (Oesterle and Elremaily 2009). The contribution of the material properties is represented by the modulus of elasticity (E) and the thermal coefficient. For concrete, E is calculated using AASHTO (2012) eq. 5.4.2.4-1; ($E_c = 33{,}000\, wc^{1.5}\sqrt{f'c}$); where the concrete unit weight (w_c) in *kcf* and the concrete compressive strength (f'_c) is in ksi. The compressive strength for a normal weight concrete superstructure component is usually 4 ksi or higher (MDOT 2013a). Typically, prestressed concrete compressive strength values are higher than 5 ksi. Modulus of elasticity for steel is 29000 ksi. The other important properties in order to complete the

analytical study are the thermal expansion coefficient and Poisson's ratio. These two properties define the way that materials deform and the magnitude of this deformation. The thermal expansion coefficient depends mainly on the properties of the aggregate that the concrete is made of (AASHTO 2012).

3.7 APPLICABLE LOADS

Loads can be applied from different design codes. In this study, loads comply with AASHTO (2012) load requirements. Particularly, loads and load combinations that are applied to design a bridge deck slab are used to design deck level connections.

3.7.1 Live Load (LL)

The AASHTO (2012) design vehicular live load is designated as HL-93. The number of lanes is the integer value obtained by dividing the clear width of the bridge deck by 12 ft. Multiple presence factors are imposed for the connection design in addition to the dynamic load allowance (IM) of 33%. AASHTO (2012) specifies that the designated HL-93 consist of the combination of:

- Design truck or design tandem, and
- Design lane load.

3.7.2 Temperature Gradient (TG) Load

Bridge decks are exposed to weather conditions more than other bridge components. Solar radiation, wind, snow, etc. result in variable deck temperatures throughout the seasons. During the day, sun radiation penetrates the deck. Since concrete has a low thermal conductivity, a non-linear divergence in temperature between the top and the bottom surfaces of the deck occurs (Branco and Mendes 1993). The highest values of positive TG happen in the summer when the temperature reaches its peak in the middle of the day. On the other hand, the lowest values of negative temperature gradient

occur in the predawn hours of the winter (Hedegaard et al. 2013). In addition to the temperature gradient profile through the depth of the superstructure, spatial variation over the bridge deck is also documented. Some TG profiles have been developed through design codes based on local field measurements of temperature, mathematical models, statistical approaches, and numerical techniques. Design specifications provide different TG profiles and equations for design purposes (Figure 22). Moreover, isothermal maps express the TG values for different regions of a country (Branco 1993). The values of T_0, T_1, T_2, T_3 are provided based on the location of the bridge. For instance, the USA is subdivided into temperature zones based on solar radiation. Each zone has a positive and a negative TG profile. The negative values are given as functions of the positive values based on the wearing surface type (i.e., plain or with an asphalt overlay) (AASHTO 2012). The temperature value at the upper surface is the highest, and decreases gradually toward the bottom of the superstructure. Similarly, the UK is subdivided into temperature zones and T_1, T_2, and T_3 differ depending on the zone. Conversely, in the New Zealand code, the temperature at the top is T_0 and the temperature value at any depth, $T_{(y)}$, decreases gradually in accordance with Priestly (1978) fifth order equation, until it reaches zero at a depth of 47.2 in., where $T_{(y)} = T_0(\frac{y}{1,200})^5$. Simplified TG profiles are provided for design purposes. The following are parameters that affect TG profiles (Elbadry and Ghali 1983; Hedegaard et al. 2013):

- Climate: solar radiation, air temperature, wind speed, and nebulosity.
- Geographical: altitude, latitude, etc.
- Time: hour of the day, day of the year, etc.
- Geometric: geometry of the cross section, bridge orientation, overlay thickness, etc.
- Material: thermal conductivity, density, specific heat, color, etc.

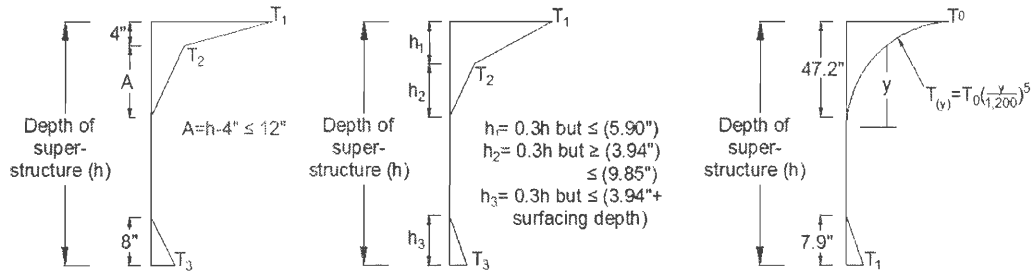

(a) AASHTO (b) British Code (c) New Zealand Code

Figure 22. TG Profile from Different Design Codes

Many studies have been performed investigating the proposed profiles of TG. Thompson et al. (1998) monitored temperature variation on the precast segmental concrete box bridge on highway US 183 in Austin, Texas. The TG values obtained were lower than the TG values in AASHTO (1994). The positive AASHTO (1994) values are the same as in AASHTO (2012), but the negative values of TG differ as a result of a change calculation method. Roberts-Wollman et al. (2002) and Hedegaard et al. (2013) carried out TG investigations. The results show that the measured positive TG is approximately the same as the TG values obtained by the fifth-order curve developed by Priestly (1978). In addition, Hedegaard et al. (2013) state that the maximum top surface measured temperature was closer to the top surface temperature provided by AASHTO (2010) for zone 2. Rodriguez et al. (2013), after a year of field monitoring of bridge temperature, found that the AASHTO (2012) TG profile is very close to the recorded TG compared to the fifth-order curve. Therefore, it can be concluded that many factors affect the TG values and for designing durable structures, local field measurements are necessary in order to have accurate values for TG. Other analytical and experimental studies have been carried out with the aim of developing temperature gradient profiles for each city in the USA. A long-term behavior monitoring of the I35 W St. Anthony Falls Bridge was carried out by French et al. (2009). They describe the full instrumentation used and include preliminary data from the monitoring. It covered the environmental impact on the bridge. The temperature gradient profile was recorded through the monitoring (Figure 23). Even though many factors influence the temperature gradients,

the study indicates that solar radiation has the highest impact on the temperature gradient profile.

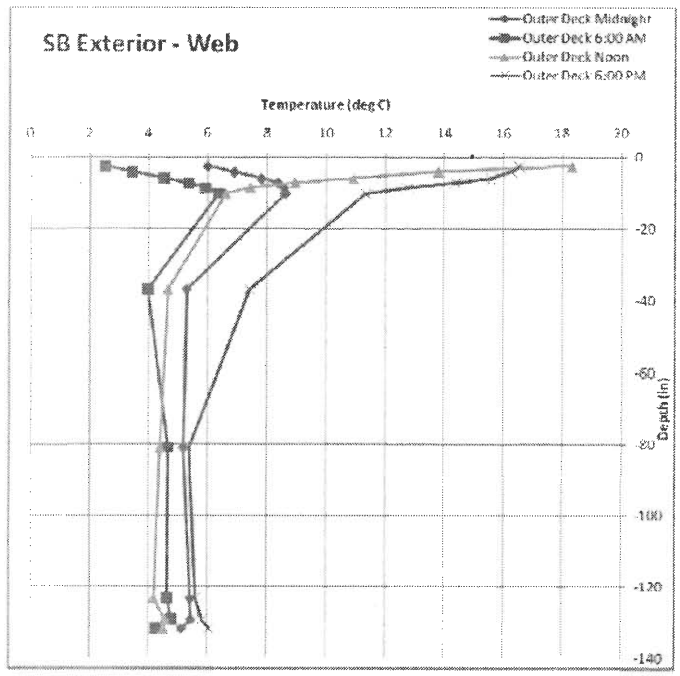

Figure 23. Thermal Gradient Profiles at Different Times of a Day (Source: French et al. 2009)

Lee (2012) investigated and evaluated the effect of weather changes throughout the year on the distribution of temperature variation in concrete girders. Initially, the study was focused on assessing the largest seasonal positive temperature gradients in bulb-tee 63 (BT-63). As shown in Figure 24, the profile of the temperature gradient is calculated by deducting the lowest temperature from the other values along the girder depth. The same procedure was repeated in 8 cities in the USA. Accordingly, a proposed temperature gradient profile was introduced (Figure 25). In a comparison with the AASHTO (2012) temperature gradient profile, the highest value of temperature is at the top and the zero value is at the top of the bottom flange of the girder.

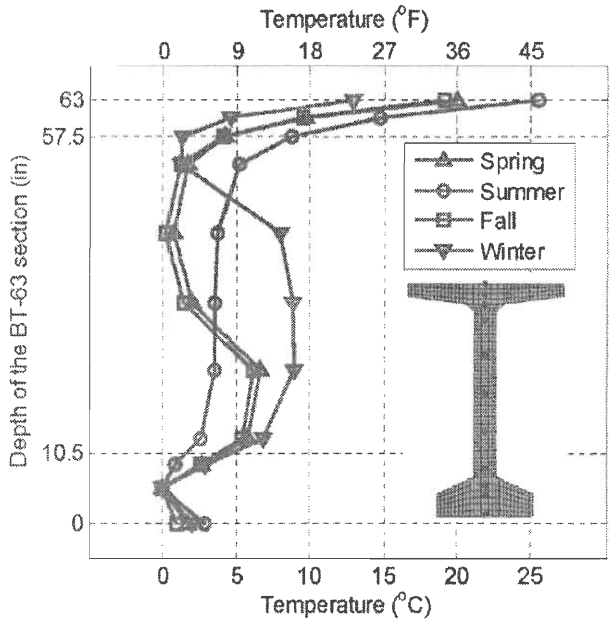

Figure 24. Largest Seasonal Vertical Temperature Gradients in BT-63 Section (Source: Lee 2012)

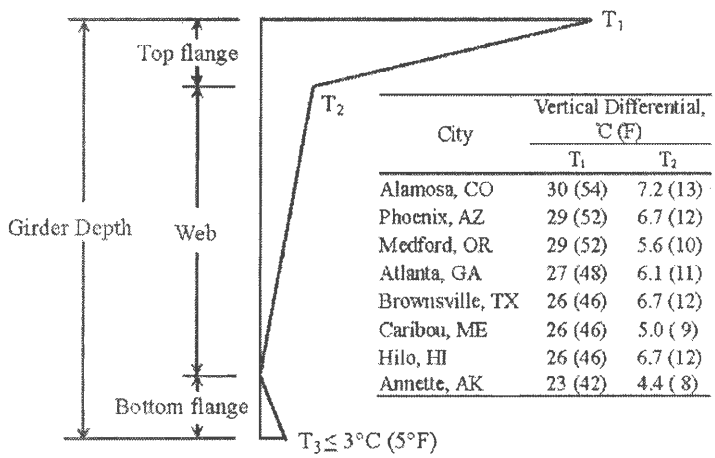

City	Vertical Differential, °C (F)	
	T_1	T_2
Alamosa, CO	30 (54)	7.2 (13)
Phoenix, AZ	29 (52)	6.7 (12)
Medford, OR	29 (52)	5.6 (10)
Atlanta, GA	27 (48)	6.1 (11)
Brownsville, TX	26 (46)	6.7 (12)
Caribou, ME	26 (46)	5.0 (9)
Hilo, HI	26 (46)	6.7 (12)
Annette, AK	23 (42)	4.4 (8)

Figure 25. Vertical Thermal Gradient of Prestressed Concrete Bridge Girders Proposed by Lee (2012)

3.7.2.1 Temperature Gradient Effect

Damage to concrete bridge decks increases due to the stresses induced by temperature (Priestly 1978, Kennedy and Soliman 1987). DeWolf et al. (1995) and Song et al. (2012) investigated the changes due to the effect of TG on the physical properties of

different systems of bridge superstructures. They concluded that of all the environmental factors, temperature variability has the greatest impact on deck deterioration. Deck condition degrades due to changes in the size and stiffness of bridges that occur with changes in ambient temperature (Mosavi et al. 2012). Deflections along the length of girders also occur with changes in temperature, causing stresses that initiate cracking (Burdet 2010). Priestly (1978) conducted his study on Auckland's New Market Bridge in New Zealand after he observed wide cracks in it. The bridge consists of prestressed concrete box girders. He found that solar radiation and ambient temperature have a main role in deteriorating the bridge deck. In the study, temperature variation in the transverse direction through the thickness of the webs of the box girders was also considered a factor that increases stresses, but was deemed insignificant. Hadidi and Saadeghvaziri (2005), reveal that environmental conditions such as temperature are the main reason for crack development. Barr et al. (2013) investigated the effect of the behavior of an integral abutment bridge and concluded that the combination of uniform temperature and TG increases stresses in the total structure (i.e., superstructure and substructure). However, Azizinamini et al. (2013) recommends that in order to mitigate the contraction and stresses induced by thermal gradient loads in bridge concrete components, aggregate with a low modulus of elasticity and thermal coefficient should be used.

CHAPTER 4

CONNECTION TYPES, LOADS, AND ANALYSIS PARAMETERS

In the previous chapter, a comprehensive review of connection types, details, and performance was carried out. Figure 28 shows a summary of the standardization process. The longitudinal connection type, the applicable loads, and the analysis parameters that will be the variables in the analytical section are introduced in this chapter. Structural analysis defines the critical analysis parameters that have a significant impact on connection load demand. The final analysis to determine the connection forces (i.e., moment, shear, and axial forces) was developed based on the critical analysis parameters, informing the design of a standardized connection.

4.1 LONGITUDINAL CONNECTION TYPE AND DETAIL

A comprehensive investigation was performed on connection details and their performance. In terms of load transfer, longitudinal connections are divided into two categories: shear and shear flexure transfer connections. The first connection type was selected to perform the load demand analysis due to good performance.

4.2 SUPERSTRUCTURE COMPONENT CONFIGURATIONS

PCI DBT and decked box beam (DBB) standard sections (Figure 2 and Figure 5) were used in the analysis. Flange thicknesses ranging from 6 in. to 9.5 in. are used by various DOTs. Hence, this flange thickness range is selected for further analysis. Girder top flange width ranges from 6 ft to 8 ft selected for further analysis. The maximum span length for each girder size was based on the 200-kip restricted span lengths in order to ensure that the chosen girder size is constructible (i.e., does not exceed lifting and transporting equipment limits).

4.3 BRIDGE GEOMETRY

This study focused on routine bridges (i.e., bridges with a span length ≤ 130 ft and skew ≤ 45°), which represent the majority of the bridges in Michigan. When the significance of the bridge length was investigated, the upper and lower limits for the span length were 130 ft and 40 ft, respectively. Bridges with 1, 2, and 3 lanes in accordance with Michigan lane and shoulder width requirements were analyzed. Bridge width was calculated with the formula (number of lanes) × (lane width of 12 ft) + (2) (shoulder width of 14ft 10 in.) (MDOT 2013b). In regards to studying the effect of skew, Michigan skew policy was applied. Therefore, skew angles of 0°, 20°, 30°, and 45° were considered.

4.4 DIAPHRAGM CONFIGURATION AND SPACING

End and intermediate diaphragm configurations and spacing, as introduced in section 3.5, were investigated. In conformity with Michigan specifications, the width of the end diaphragms for the DBT and DBB bridge systems was 8 in. and 24 in., respectively. Also, the width of the intermediate diaphragms was 8 in. and 14 in, respectively for the two bridge systems (MDOT 2013b). DBB intermediate spacing was as listed in Table 1. DBT intermediate diaphragm spacing was:

- One or no diaphragm for span ≤ 80 ft,
- Two diaphragms at 1/3 points for 80 < span ≤ 120 ft, and
- Three diaphragms at 1/4 points for span > 120 ft.

Table 1. DBB Intermediate Diaphragm Spacing (Source: MDOT 2013b)

Span length	Location
Up to 50'	2 at center of span (11' apart)
Over 50' to 62'	1 at center of span and 1 at each quarter point
Over 62' to 100'	2 at center of span (11' apart) and 1 at each quarter point
Over 100'	5 equally spaced between

4.5 MATERIAL PROPERTIES

Material properties were in accordance with AASHTO (2012) and MDOT (2013a). The concrete properties were: a compressive strength of 5 to 7 ksi, a thermal expansion coefficient of 6×10^{-6} /°F and Poisson's ratio of 0.2. However, due to the high bond strength and ductility of UHPC, its use was also taken into consideration. UHPC has a 20 ksi compressive strength, 7200 ksi modulus of elasticity, and 8.2×10^{-6} /°F thermal expansion coefficient (Ductal JS 1000).

4.6 LOADS

Values of TG and LL that comply with AASHTO (2012) and MDOT (2013a) specifications were selected for analysis. Michigan is located in zone 3 of the US Isothermal Map. Figure 26 (a) and (b) show the positive temperature gradient (PTG) profile and the negative temperature gradient (NTG) for concrete superstructures. The analysis was based on the use of plain concrete decks, thus the negative temperature gradient profile was determined by multiplying the positive temperature values by -0.3. Dead load due to girder self-weight has no contribution to the longitudinal connection load demand since connections are cast after the girders are erected. Therefore, dead load effect was not taken into consideration. MDOT (2013a) requires that live loads are as designated in AASHTO (2012), with the exception that the design tandem is replaced with a single 60 kip load (Figure 27). Wheel load stresses shown in Figure 27 are calculated based on a 20 in. × 10 in. tire contact area. However, for Michigan interstate and trunkline bridges, vehicular live loading designated as HL-93 Mod shall consist of 1.2 times the combination of the:

- Design truck (HL-93 truck) or 60 kip single axle load and
- Design lane load (0.64 klf).

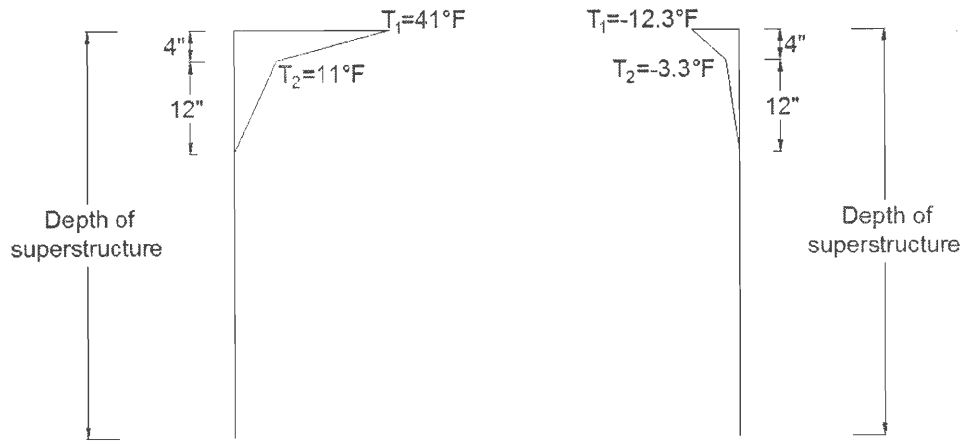

(a) Positive Temperature Gradient (PTG) (b) Negative Temperature Gradient (NTG)

Figure 26. AASHTO (2012) Temperature Gradient Profile Zone 3

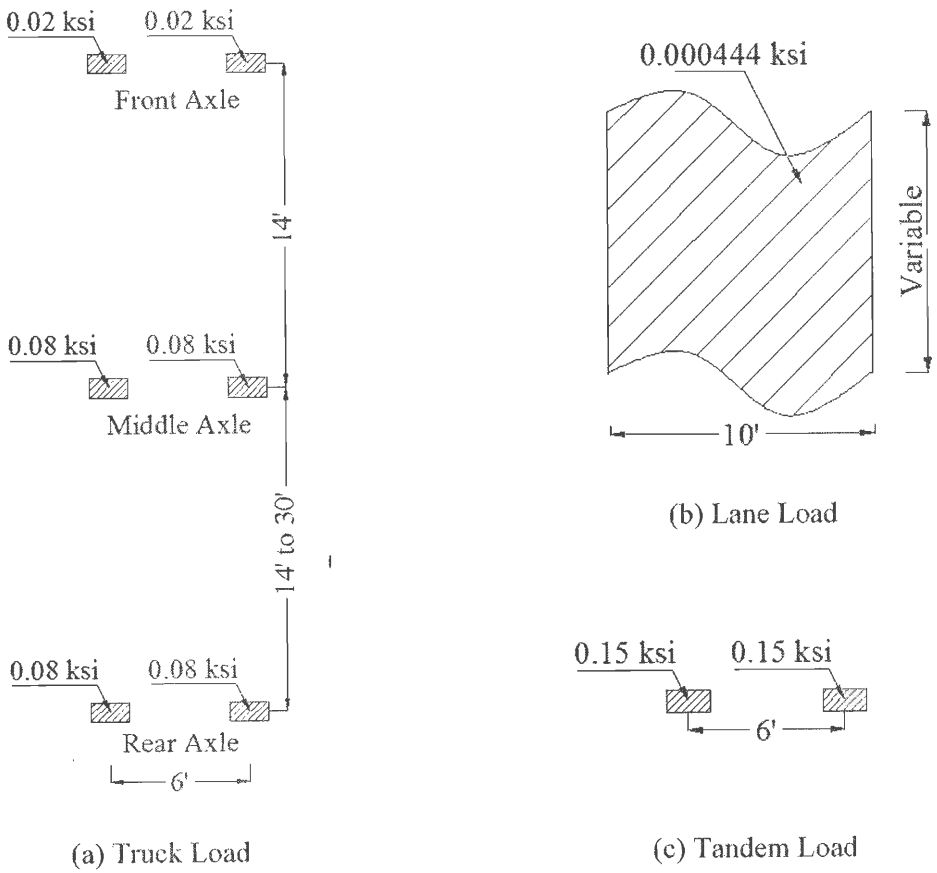

(a) Truck Load (b) Lane Load (c) Tandem Load

Figure 27. HL-93 Mod Load

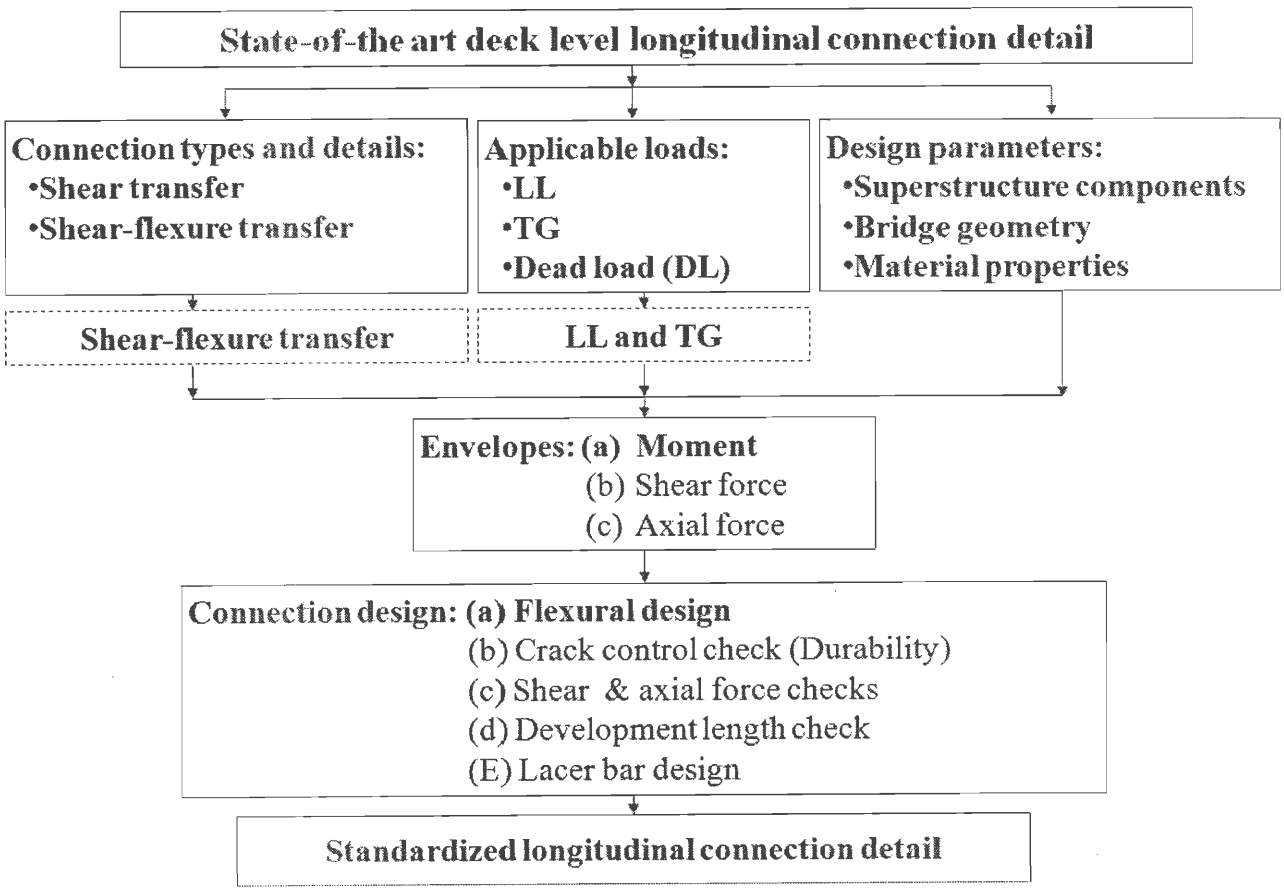

Figure 28. Connection Standardization Process

CHAPTER 5

CONNECTION LOAD DEMAND CALCULATION

The moments and forces developed at the longitudinal connection were calculated using finite element (FE) bridge models. As the first step in the process, the effect of TG in conjunction with the design parameters listed in the previous chapters was evaluated. The critical parameters that produce the highest load demand at the connection were identified. Afterward, the final analysis models were developed incorporating LL and TG to obtain moment and force envelopes to be used for designing the standardized connection details.

5.1 STRUCTURAL MODELING AND ANALYSIS

Temperature gradient analysis is complicated and requires the use of advanced programs. The analysis was performed by modeling simply supported single span three dimensional (3D) finite element (FE) bridge models. FE models were developed using Abaqus version 6.12.2 (Abaqus 2012). The three major components of bridge superstructure that were included in the models are girders, longitudinal connections, and intermediate and end diaphragms. All the components were modeled using 3D eight-node solid elements (C3D8). The longitudinal connections were the component that was of greatest interest. Therefore, sensitivity analysis was carried out on this component in order to obtain accurate results.

Two sizes of DBT and one size of DBB FE models were analyzed to evaluate the significances of the design parameters in conjunction with TG. The impact of a parameter on the connection load demand was evaluated using DBT models by varying one parameter at a time while keeping the other parameters unchanged. Once the significance of each design parameter was clarified from DBT FE models, DBB models were analyzed to give a comprehensive understating of the design parameter impacts.

5.1.1 Decked Bulb-T and Decked Box-Beam Girder Models

PCI standard DBT sections were used. In order to ensure a good mesh quality for the FE analysis, section configurations were slightly changed by altering the taper at the top flange to the web connection of the DBT section (Figure 29) and the internal corners of the DBB section (Figure 30). However, this change resulted in negligible difference in the section properties.

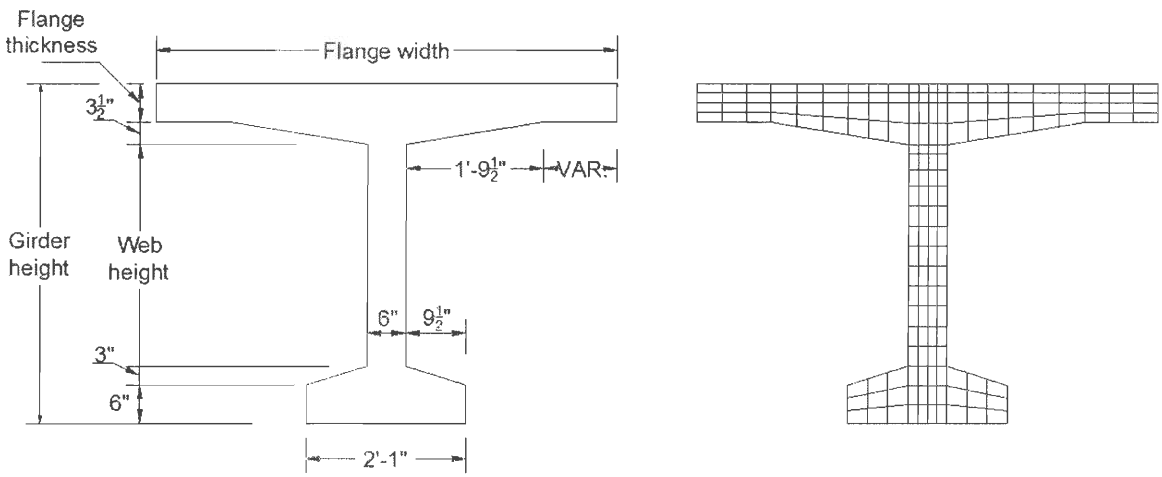

Figure 29. Modified DBT Section and the FE Mesh

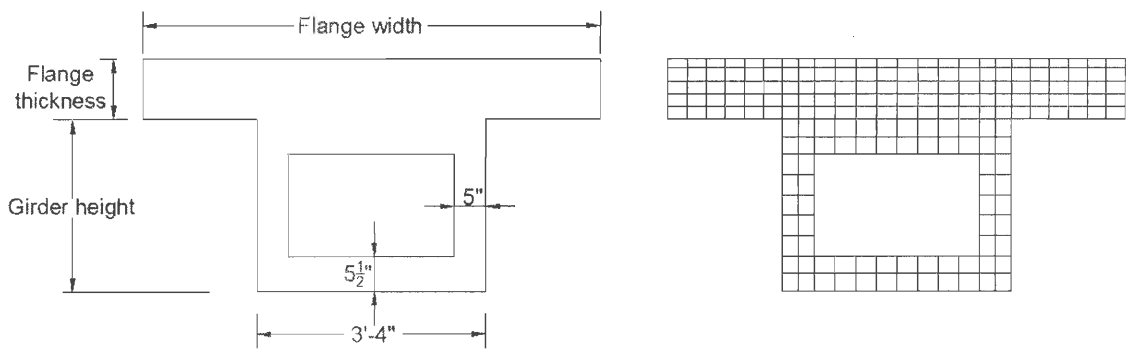

Figure 30. Modified DBB Section and the FE Mesh

5.1.2 Two-DBT-Girder Model

The two-DBT-girder model in Figure 31 was used to evaluate the impact of the design parameters by incorporating one parameter at a time. It was then analyzed under the TG load. This model was mainly used to verify the TG modeling.

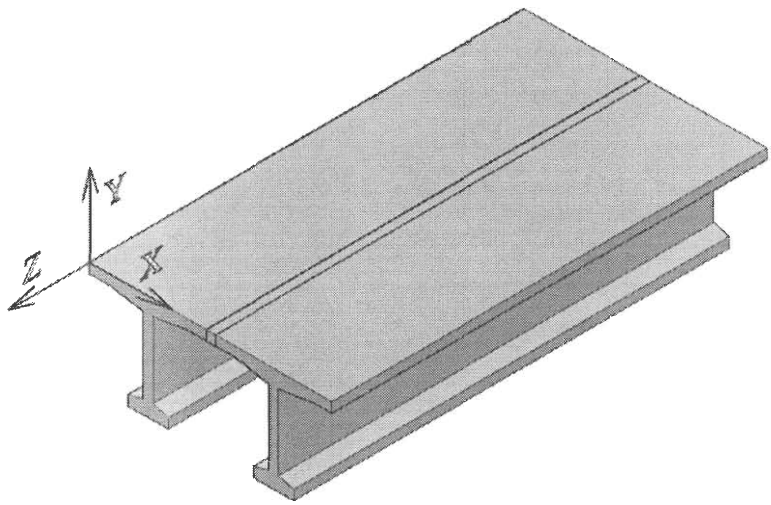

Figure 31. Two DBT Girder Model

5.1.3 Full DBT Bridge Model

A full bridge model (Figure 32) was analyzed to evaluate the influence of most of the design parameters on connection load demand. Once the influence of all these parameters was assessed, and in order to calculate the final connection load demand envelopes, a seven girder final model was developed and analyzed.

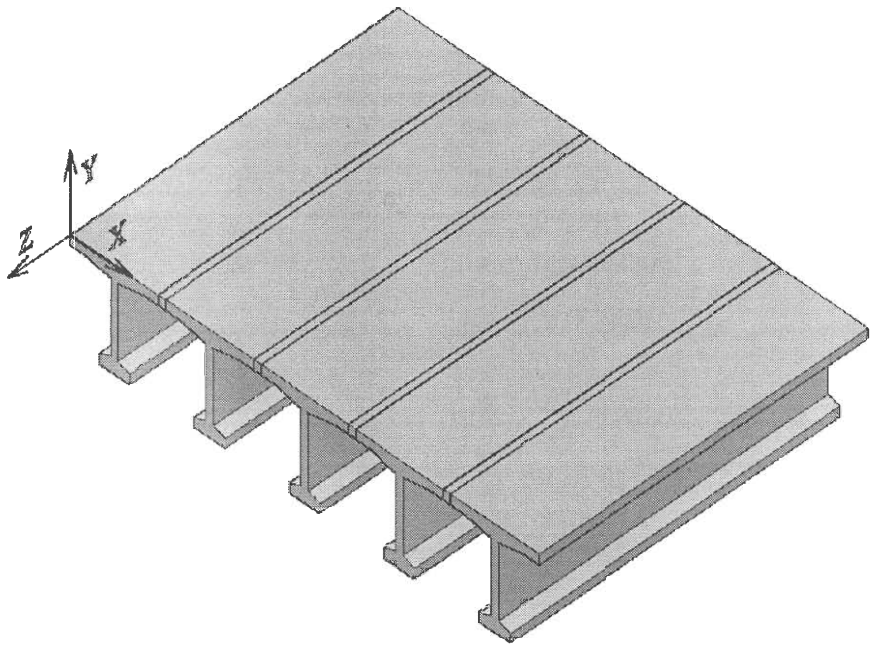

Figure 32. Full DBT Girder Model

5.1.4 Full DBB Bridge Model

This model was used for the evaluation in the same way as the previous model. Figure 33 shows the full DBB model that consisted of 5 girders and was used to assess the aforementioned design parameters.

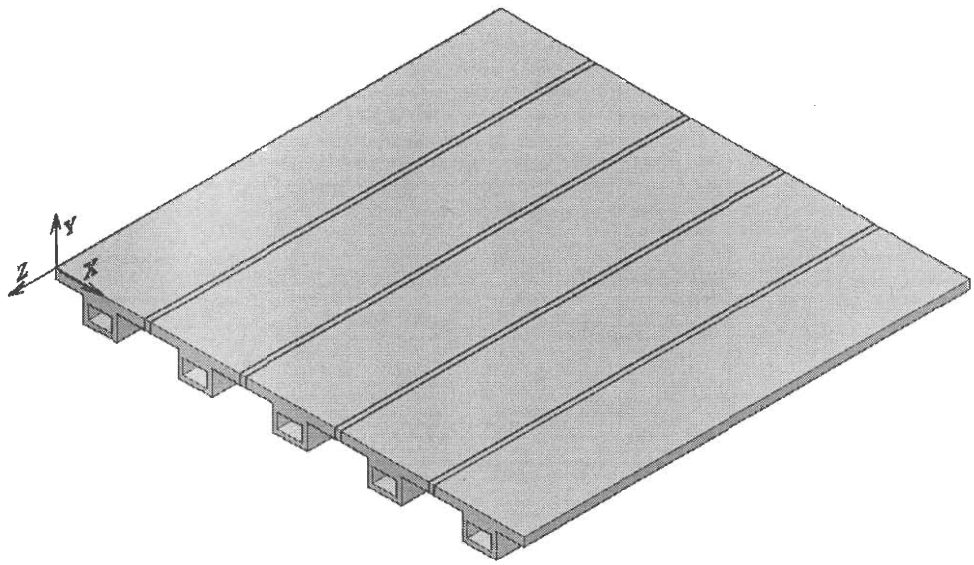

Figure 33. Full DBB Girder Model

5.2 BOUNDARY CONDITIONS

Roller and pin supports were assigned to the models. Both support types consisted of main and secondary nodes (Figure 34). The main nodes in the pin supports were restrained from moving in the three directions (x, y, and z). The secondary nodes in the pin supports were restrained from moving in two directions (y and z). On the other hand, the main nodes in the roller supports were restrained from moving in two directions (x and y) and the secondary nodes were restrained from moving in only one direction (y).

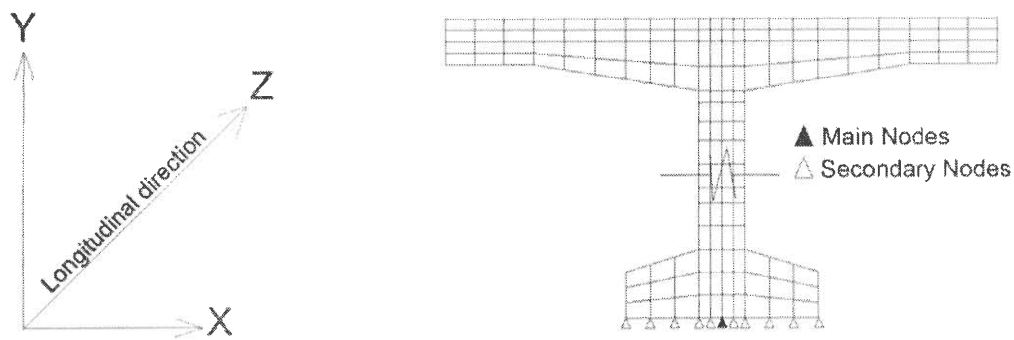

(a) Main Axis in a 3D View (b) Main and Secondary Node Locations

Figure 34. Boundary Conditions

5.3 LOAD APPLICATION

Live load was applied as pressure. The tire contact area of 10 in. × 20 in. was considered. The TG was applied by assigning a certain temperature value to a layer of nodes at a certain depth from the top surface of the girders. In an example shown in Figure 35, when TG zone 3 is considered, the node layer at the top surface of the girder will be assigned a temperature value of 41° F, and the node layer at 16 in. from the top of the girder will be assigned 0° F. However, a node layer at a level 4 in. from the top will be assigned a temperature value of 11° F, the node layers at a level *y* in. from the top will be assigned a temperature value of $T1_{(y)}$ or $T2_{(y)}$ where:

$$T_{1(y)} = \frac{30(4-y)}{4} + 11 \text{ ; If } 4 \text{ in.} > y > 0 \text{ in.}$$

$$T_{2(y)} = \frac{11(16-y)}{12} \text{ ; If } 16 \text{ in.} > y > 4 \text{ in.}$$

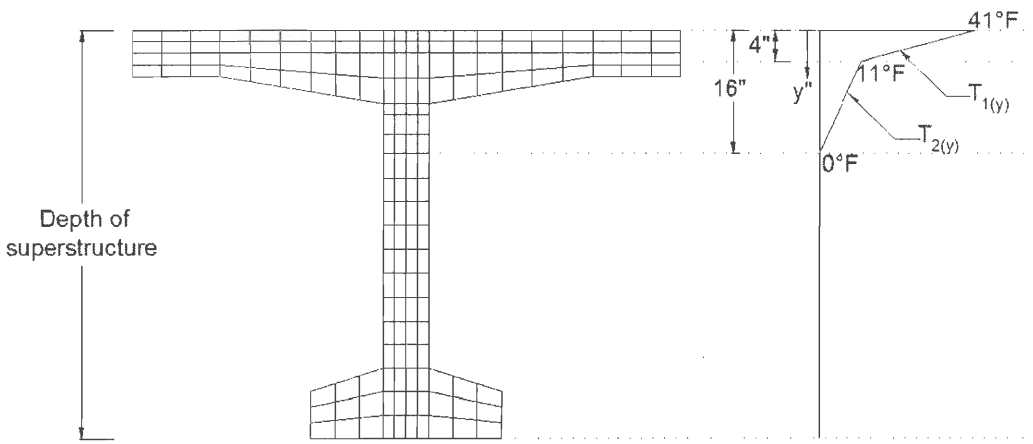

(a) Meshed Girder (b) PTG zone 3

Figure 35. TG Application to Node Layers at Different Levels of Depth

5.4 MODELING VERIFICATION

The two-DBT-girder model was utilized to verify the modeling method (Figure 36). The model consisted of two DBT-65 girders with total length of 100 ft. The width of the top flange of each girder was 6 ft connected with a 6 in. wide joint. An arbitrary static linear load of 0.001675 kip/in. was applied at the mid-distance between the two girders. To simplify the calculations: (1) the three nodes (L, C, and R) along the bottom flange width were restrained at each end of the two girders and (2) diaphragms were not included.

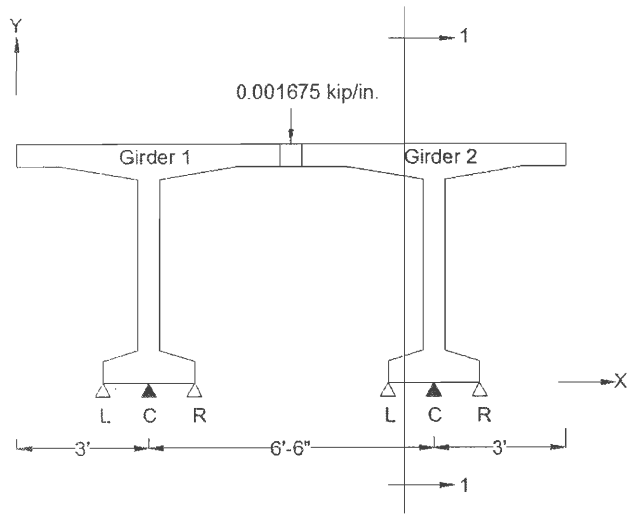

(a) Cross section

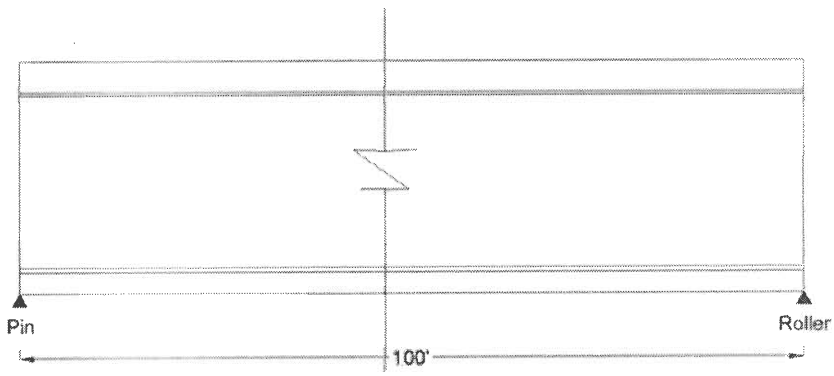

(b) Section (1-1)

Figure 36. Verification Model Geometry and Static Load

Table 2. Girder 1 Reactions Resulted from the Applied Static Load

Node	Pin			Roller		
	R_X	R_Y	R_Z	R_X	R_Y	R_Z
L	0	0.1039	-0.0301	0	0.0983	0
C	0.03251	0.3155	-0.0101	0.0246	0.3137	0
R	0	0.0830	0.0402	0	0.0904	0
$\sum$	0.0325	0.5025	0	0.0246	0.5025	0

Table 3. Girder 2 Reactions Resulted from the Applied Static Load

Node	Pin			Roller		
	R_X	R_Y	R_Z	R_X	R_Y	R_Z
L	0	0.1039	-0.0301	0	0.0983	0
C	-0.03251	0.3155	-0.0101	-0.0246	0.3137	0
R	0	0.0830	0.0402	0	0.0904	0
$\sum$	-0.0325	0.5025	0	-0.0246	0.5025	0

The reactions at each girder support that resulted from the applied load are given in **Table 2** and Table 3). Moment and shear results in the middle of the connection were obtained by defining a Free Body in Abaqus. The moment and shear values for the total section of the connection were 36.011 in.-kip and 1.005 kip, respectively. The same values can be calculated from the support reactions. It should be noted that in Figure 37, a reaction value in a certain direction is the summation of the reaction values at the pin and roller supports of one girder. For instance, the vertical reaction of girder 1 at node C equals the reaction at node C of the pin support plus the reaction of node C at the roller support (0.3155 + 0.3137 = 0.629 kips). The equilibrium check for the total structure was conducted as follows.

$\sum f_x = 0$, 0.0571- 0.0571= 0 kip

$\sum f_y = 0$, 1.005 + 1.005 - 0.001675 (1200) = 0 kip

$\sum M_{@\ \text{connection center}} = 0$, 36.011 - 36.011 = 0 in.-kip

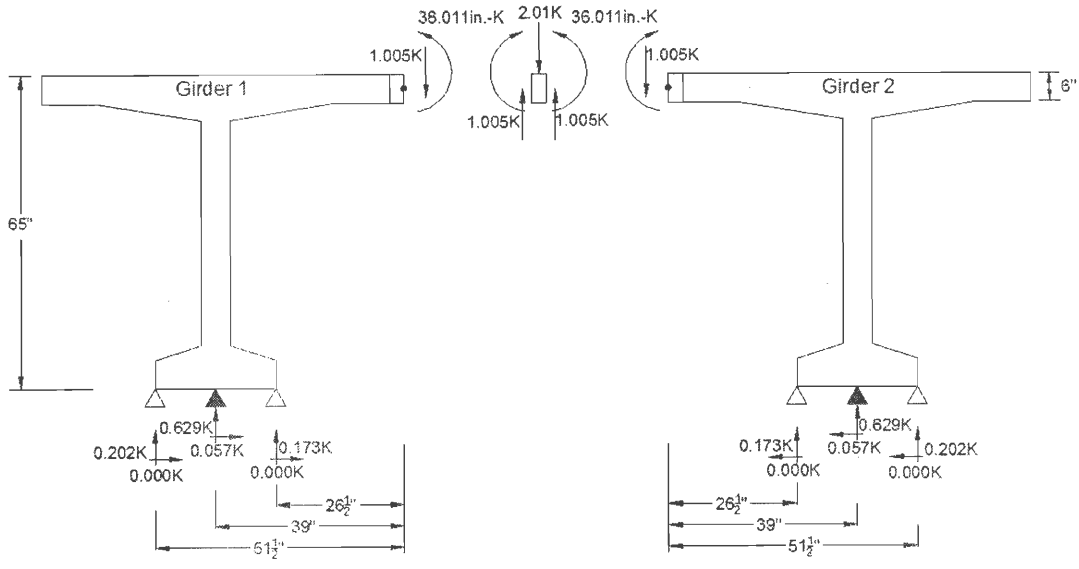

Figure 37. Verification Model Results due to the Static Load

5.5 EFFECT OF DESIGN PARAMETERS ON CONNECTION LOAD DEMAND

The assessment of the impact of every design parameter in conjunction with TG was performed. Connection internal forces generated due to NTG are small relative to the forces due to PTG. Therefore, the study was performed using the PTG load. Appendix A provides the analysis results. The stress resultants (i.e., moments and forces) were calculated at the connections under the TG load due to the external and internal constraints in the structure. The external constraints in the transverse direction are formed as a result of the boundary conditions. On the other hand, the internal constrains develop due to the profile of the temperature along the depth of the superstructure. The axial forces that are generated at the connection due to the PTG are in compression. Thus, the flexural moments developed at the connection were considered for the evaluation and design.

Table 4 presents a summary of the analysis results, where the comparison was based on DBT FE model results. The percent change in the flexural moment was calculated using the moments developed at the connection when the maximum and minimum values of the design parameter were assessed. For example, 40 and 130 ft were

used as the minimum and maximum span lengths to compare the effect of increasing the bridge span length. As shown in the first row of Table 4, there is a 5% reduction in the moment value of 130 ft span length when compared to the 40 ft span. On the other hand, there is a significant increase in the moment value when the flange thickness increases. An increase in the number of internal diaphragms and the modulus of elasticity of girders has a considerable effect on the connection moments. Likewise, when the joint is made of UHPC the moment value increases due to the increase in both the modulus of elasticity and the thermal coefficient. The effect of some design parameters such as girder size and diaphragm spacing on DBB bridge system can differ. Therefore, TG analysis was conducted on DBB FE models and the results are presented in Table 5.

Table 4. The Effect of the Design Parameters on the DBT Longitudinal Connection Moment under the PTG

Design Parameters	Percent change in transverse flexural moment at the connection
Increase in bridge length from 40 ft to 130 ft	-5
Increase in bridge width from 42 ft to 66 ft	≈0
Increase in skew from 0° to 45°	-5
Increase in girder spacing from 6.5 ft to 8.5 ft	-5
Increase in girder depth from 35 in. to 65 in.	+5
Increase in flange thickness from 6 in. to 9.5 in.	+128
Increase in the girder modulus of elasticity from 4287 ksi to 5072 ksi)	+13
Increase in the connection material modulus of elasticity from 4287 ksi to 5072 ksi	+5
Increase in the diaphragm concrete modulus of elasticity from 4287 ksi to 5072 ksi	+1
Use of UHPC for connections: increase in E from 4287 ksi to 7200 ksi and α from 6.0×10^{-6} /°F to 8.2×10^{-6} /°F	+17
Use of full depth end diaphragms from partial depth to full depth	+6
Increase in the intermediate diaphragm depth from partial depth to full depth	+6
Decrease in intermediate diaphragm spacing from no in-diaphragm to 3 in-diaphragms	+33

Table 5. The Effect of the Design Parameters on the DBB Longitudinal Connection Moment under the PTG

Design Parameters	Percent change in flexural moment
Increase in girder width from 3 ft to 4 ft	+9
Increase in a bridge span length from 40 ft to 63 ft accompanied with increase in the number of intermediate diaphragm	-2

However, TG forces a bridge to deform in the horizontal direction, which can be excessive, and lead to crack development. Therefore, in the parametric study the expansion that occurs in the bridge width due to TG was evaluated. As shown in Figure 38, when a bridge length increases the horizontal deformation increases. AASHTO (2012) states upper limits for deflection that can occur in bridges. The maximum horizontal deflection for each span length due to TG does not exceed the upper limit when live load deflection limit is taken into consideration (Table 6). It was considered that the middle line of the bridge width is the origin for measuring deflection. Therefore, it should be noted that bridge horizontal deflection in Table 6 is half the deflection values shown in Figure 38.

Table 6. Horizontal Deflection in a Bridge Width due to TG Compared to the Maximum Deflection Criteria

Bridge Span Length (ft)	Maximum Allowable Deflection (Span/800) (in.)	Bridge Horizontal Deflection (in.)
40	0.60	0.029
70	1.05	0.032
100	1.50	0.036
130	1.95	0.040

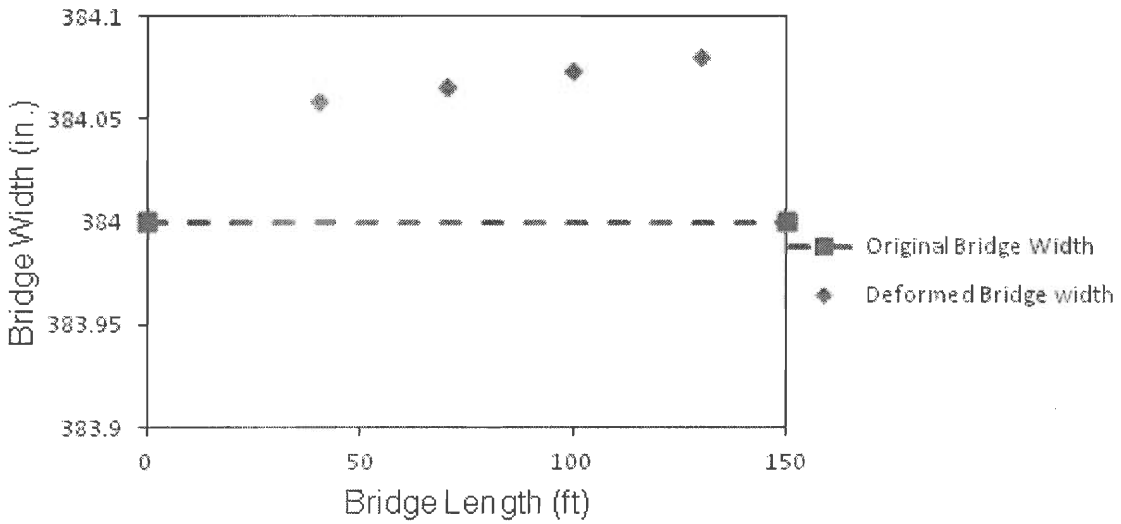

Figure 38. The Increase in a Bridge Width due to TG.

The information presented in Table 4 and Table 5 is depicted in Figure 39, which can be considered the decision chart for developing the final analysis models for the two DPPCG bridge systems. The final bridge models are intended to develop the highest moment demand at the connection under the TG and the LL. Therefore, the final models can be considered standard models for a longitudinal connection design.

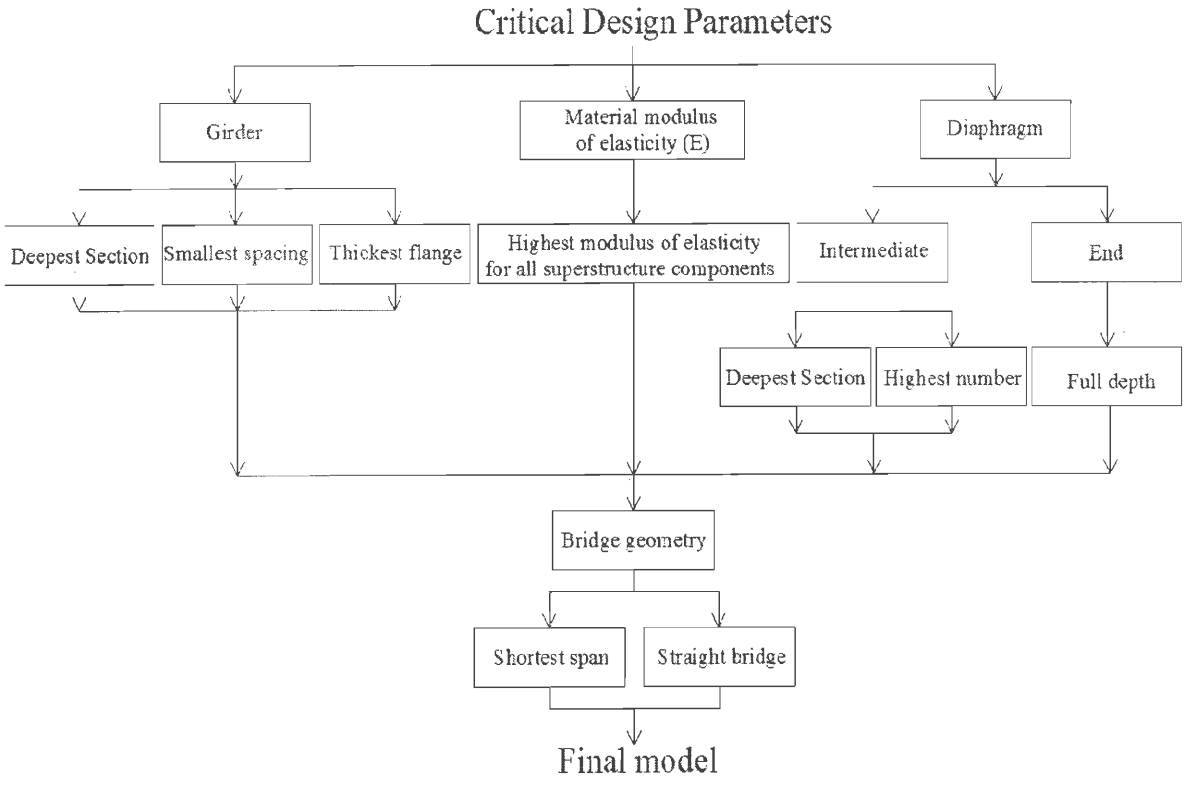

Figure 39. Decision Chart for Developing Final DBT Analysis Model

Figure 39 illustrates the design parameters that maximize the connection load demand for a DPPCG bridge system. However, there is a contradiction between using the deepest girder section and the shortest span length. As shown in Table 5, when the bridge span length increases, the flexural moment decreases by 5%. When the deepest girder is used, the flexural moment increases by 5%. Thus, using an appropriate section size for the final bridge model with the shortest span is justified. From Table 5, the reduction in the moment value as a result of an increase in the girder spacing from 6.5 ft to 8.5 ft is 5%. ASHTO (2012) Table A4-1 shows that the flexural moment due to the LL increases by approximately 20% when the spacing between girders is 8.5 ft. Hence, considering the girder spacing impact on LL moments at the connection, 8.5 ft spacing was selected for the final models. Likewise, the widest girder section causes the highest connection load demand (Table 5).

5.6 FINAL BRIDGE MODELS

Two simply supported single span, multilane bridge models were developed once the significance of the design parameters on the connection load demand under TG was clarified. These FE models encompassed the critical design parameters identified from the previous analysis. The final analysis incorporated the LL and TG. Bridge width has a negligible influence on the connection moment when TG is applied (Table 4). Two lanes of Michigan lane and shoulder widths were considered in designing a prototype for calculating the connection moments and developing the design details. One freeway lane was 12 ft wide and one shoulder was 14 ft 10 in. wide (MDOT 2013b). Hence, the two final 3D bridge models were 40 ft long and 59 ft wide. The first model consisted of seven DBT-35 girders (Figure 40) and the second of seven DBB-I-48 girders (Figure 41). In the two models, the width of each girder was 8 ft and the flange thickness was 9.5 in. The longitudinal connection was 6 in. wide. The analysis included the PTG, NTG and LL. Table 7 shows the final analysis results.

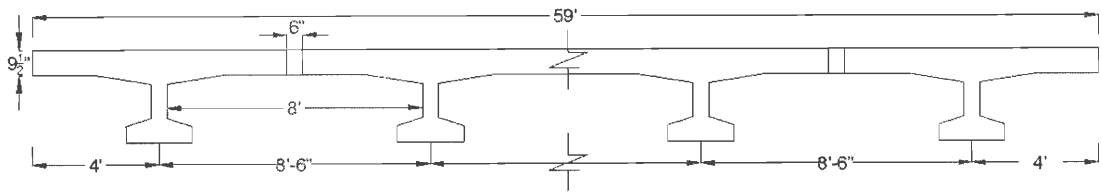

Figure 40. Final DBT FE Model

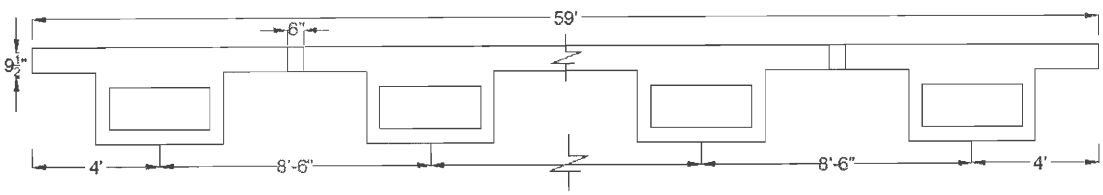

Figure 41. Final DBB FE Model

Table 7. Load Demand at the Longitudinal Connection in DBT and DBB Bridge Models Due to LL, PTG and NTG

Load	Moment, M (ft-kip/ft)		Shear force, V (kip/ft)	
	DBT	DBB	DBT	DBB
LL	+13.0 -2.0	+6.0 -0.6	5.7	5.0
PTG	+10.0	+9.3	-	-
NTG	-3.0	-2.8	-	-

LL generates a higher moment than the PTG in DBT. On the other hand, PTG moment is higher than LL moment in DBB. The LL moment in DBT is larger than the LL moment in DBB because of the clear spacing between girders. For instance, the clear spacing between two girders equals the girder spacing minus the girder web width. Thus in DBT, the clear spacing is 8.5 ft – 0.5 ft = 8 ft; and in DBB, the clear spacing is 8.5 ft – 4 ft = 4.5 ft. The positive moments due to TG are equivalent for both systems. Similarly, the negative moments due to TG are equivalent for both systems.

CHAPTER 6

CONNECTION DESIGN

According to the literature review and structural analysis that were carried out on the longitudinal connection, it was decided to design a shear-flexure transfer connection. This was selected due to: (1) its ability to provide full continuity between neighboring girders and thus transfer both shear and moment, and (2) its superior performance record. Particularly, a U-bar connection detail was designed because it can provide an adequate resistance against crack development and promote long-term durability. The forces taken into account in the design were determined by applying TG and LL to the final DBT bridge model (Table 7). The connection was designed with normal concrete and mild reinforcement. Conventional concrete design procedures, in accordance with AASHTO (2012) and MDOT (2013 a and b) specifications, were followed. Flexural reinforcement that satisfies the maximum moment at strength limit state was designed and crack control criteria was checked. Other checks, such as development length and shear capacity of the section, were performed. Lacer bars design was performed as well. The step by step design of a DBT connection and a DBB connection is provided in appendices B and C, respectively. Connection details are provided. The following variables used in the design are:

- Structural connection thickness = 9 in.
- 28-day concrete compressive strength, (f'_c) = 7 ksi,
- Elastic modulus of concrete (E_c) = 5,072 ksi
- Yield strength of reinforcement (f_y) = 60 ksi,
- Elastic modulus of reinforcement (E_s) = 29,000 ksi
- Modular number (n) = 6
- Bottom concrete cover = 1.5 in. from the centerline of the bottom layer of reinforcement
- Top clear concrete cover = 3 in.

6.1 PROPOSED CONNECTION CONFIGURATION

The connection geometry is female-to-female 6 in. wide shear key (Figure 42). The proposed configuration of the connection was intended to complete the standardization process. Different factors such as the bonding strength of the connection material and the interface shear failure pattern can change the shear key shape.

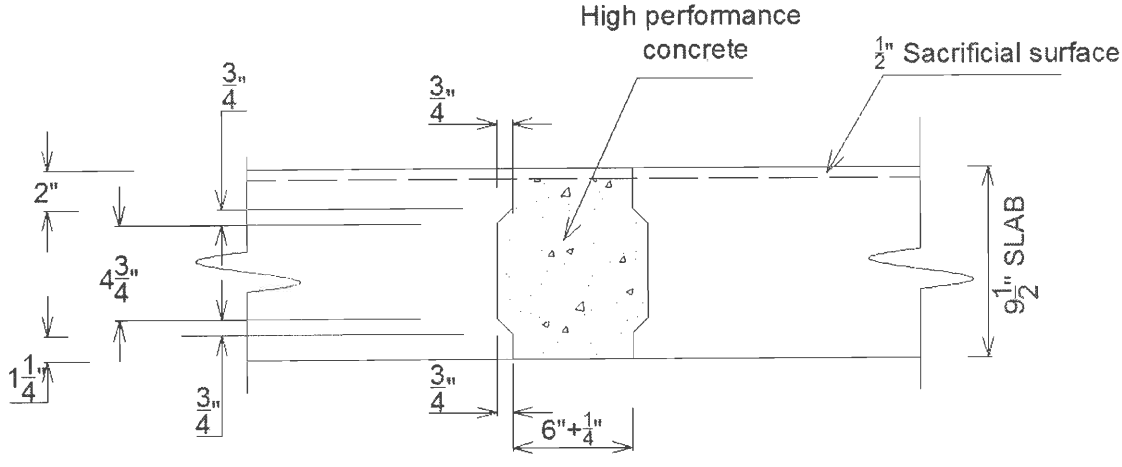

Figure 42. Proposed Longitudinal Connection Configuration

6.2 MOMENT LOAD COMBINATIONS

Load combinations in accordance with AASHTO (2012) table 3.4.1.-1 are utilized:

Strength I:

- Positive moment $M_{STI\text{-}P}$: 1.75(positive LL moment) = 22.75 ft-kip/ft
- Negative moment $M_{STI\text{-}N}$: 1.75(negative LL moment) = -3.3 ft-kip/ft

Service I:

- Positive moment $M_{SI\text{-}P}$: The greatest of

  1.0 (positive LL moment+0.5 PTG moment) =18 ft-kip/ft → $M_{SI\text{-}P}$ =18 ft-kip/ft

  1.0 (PTG moment) =10 ft-kip/ft
- Negative moment $M_{SI\text{-}N}$: The greatest of

  1.0 (negative LL moment+0.5 NTG moment) =3.4 ft-kip/ft → $M_{SI\text{-}N}$ =-3.4 ft-kip/ft

1.0 (NTG moment) =-3 ft-kip/ft

6.3 FLEXURAL DESIGN

The required amount of flexural steel (A_s) was calculated for the positive moment ($M_{STI\text{-}P}$ = 22.75 ft-kip/ft) as A_s = 0.7 in^2/ft. Therefore, #5 bars @ 5 in. satisfy the required area of steel. Due to the concrete cover requirement, the top reinforcement is located at 3 in. below the top surface. The neutral axis of the section is located at 0.9 in. below the top surface. Hence, the top reinforcement is located within the tension zone. The strain in the top reinforcement is calculated as 0.008, which is greater than the yield strain of steel. Economically, the section should be redesigned using both layers, resulting in a requirement of 0.99 in^2/ft of steel. Therefore, it is recommended to reinforce the connection with #5 bars @ 7 in.

6.4 CONTROL OF CRACKING BY DISTRIBUTION OF REINFORCEMENT

Long-term durability necessitates well-distributed reinforcement that is capable of limiting crack width. AASHTO (2012) eq. 5.7.3.4-1 is used as an upper limit for steel reinforcement spacing to control crack development in a concrete component. Therefore, the spacing of mild steel reinforcement in the layer closest to the tension face shall not exceed S. Where,

$$S = 700\frac{\gamma_e}{\beta_s \cdot f_{ss}} - 2d_c \quad ; \quad \beta_s = 1 + \frac{d_c}{0.7(h - d_c)}$$

where,

γ_e = an exposure factor (i.e., 1 for class exposure 1 or 0.75 for class exposure 2)

d_c = thickness of concrete cover measured from center of the reinforcement (in.)

f_{ss} = tensile stress in steel reinforcement at the service limit state (ksi).

h = component total structural depth (in.).

d_t = distance from extreme compression fiber to the centroid of the extreme tension reinforcement (in.).

Equation 5.7.3.4-1 was developed based on the assumption that crack width does not exceed 0.017 in. The exposure factor (γ_e) is used to control the maximum expected crack width. That is, if the concrete component is exposed to sever conditions, the exposure factor can be assumed to lower than 0.75. β_s factor is "*a geometric relationship between the crack width at the tension face versus the crack width at the reinforcement level*" AASHTO (2012). The reinforcement spacing is 7 in. when #5 bars are used. Steel stress, f_{ss} = 58.75 ksi, and β_s=1.28. Assuming exposure 2 condition (i.e., γe= 0.75), Therefore,

$$S \leq 700\frac{\gamma_e}{\beta_s \times f_{ss}} - 2d_c \quad = 700 \times \frac{0.75}{1.28 \times 58.75} - 2 \times 1.5 = 3.9 \text{ in.} < 7 \textit{ in.}$$

As shown in the above equation, the condition is not satisfied. The tensile stress in the steel reinforcement (f_{ss}) is close to the yield strength of the steel. Therefore, the design is revised by changing the bar size. If #4 is bar used, the reinforcement is #4 @ 4 in. This results in S= 4.7 in., which is greater than 4 in. and the condition is satisfied. Yet, the steel stress (f_{ss}) is very high at 53 ksi, which is around 90% of the steel yield strength. For service limit states, this value seems unacceptable. The AASHTO (2012) eq. 5.7.3.4-1 does not have an upper limit to the tensile stresses (f_{ss}). The original sources for this equation Frosch (2001) and DeStefano et al. (2003) limit f_{ss} to 80% of steel yield strength. Hence, the detail was revised to #4 @ 3.5 in., which resulted in steel stress of 47 ksi, less than 80% of fy. It is recommended to use #4 @ 3.5 in. U bars for the connection. The flexural reinforcement is staggered in relation to adjacent girders. Accordingly, in order to accomplish the reinforcement require for the connection, #4 @ 7 in. U-bars shall be distributed in each girder flange (Figure 44).

6.5 CRACKING MOMENT CAPACITY

In accordance with AASHTO (2012) articles 5.4.2.6 and 5.7.3.6.2, the cracking moment capacity of the section was calculated as 8.6 ft-kips/ft, which is greater than the negative moment at service limit state (i.e., $M_{SI-N} = 3.4 \text{ ft} - \text{kip/ft}$). Thus, the section

capacity is sufficient to prevent top surface cracking due to the negative moment. In general, the bond strength at the interface is much lower than the concrete tensile strength (Aktan et al. 2009). The weak bond strength was not considered in calculations of cracking moment capacity. A much lower cracking capacity is expected and requires evaluating the bond strength of the material used in forming the connections.

6.6 SHEAR CAPACITY

Shear capacity of the section was checked in accordance with AASHTO (2012) article 5.8.3.3. Concrete shear capacity of a one-foot section at the connection is 8.6 kip/ft, which is less than the shear demand of 10 kip/ft at strength-I. Shear capacity from the flexural reinforcement was calculated to check the total section capacity. The total shear section capacity is 97.3 kip/ft, which is greater than the shear demand. Therefore, the connection is capable of developing an adequate shear capacity.

6.7 DEVELOPMENT LENGTH

The development length (L_d) consists of the 6 in. between the U-bar bearing surfaces (Figure 43). As per the AASHTO (2012) article 5.11.2.1 the development length requirement was satisfied.

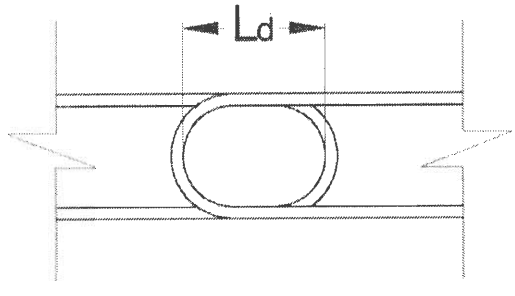

Figure 43. Development Length Detail

6.8 LACER BAR DESIGN

To determine the appropriate size of lacer bars, He et al. (2013) equation was used:

$$\frac{A_{lbar}.f_{y,lbar}}{A_{ubar}\,f_{y,ubar}} \geq \frac{S}{4L_d}$$

where,

A_{lbar} = the area of one lacer bar

A_{ubar}= the area of one U-bar (i.e., the area of the two legs)

$f_{y,lbar}$ = yield strength of the lacer bars

$f_{y,ubar}$ = yield strength of the U bars

S= the spacing between the u bars

L_d= the development length

If the yield strength of the lacer bars is the same as the yield strength of the connection reinforcement, and the connection is reinforced with #4 @ 7in. spacing, the lacer bar diameter should not be less than 0.385 in. It is recommended to use #4 lacer bars for the connection.

6.9 STANDARDIZED LONGITUDINAL CONNECTION DETAIL

Figure 44 and Figure 45 show the standardized connection detail for the longitudinal connection. The detail is for longitudinal connections in DBT and DBB bridge systems. Tolerances in construction are included in the details.

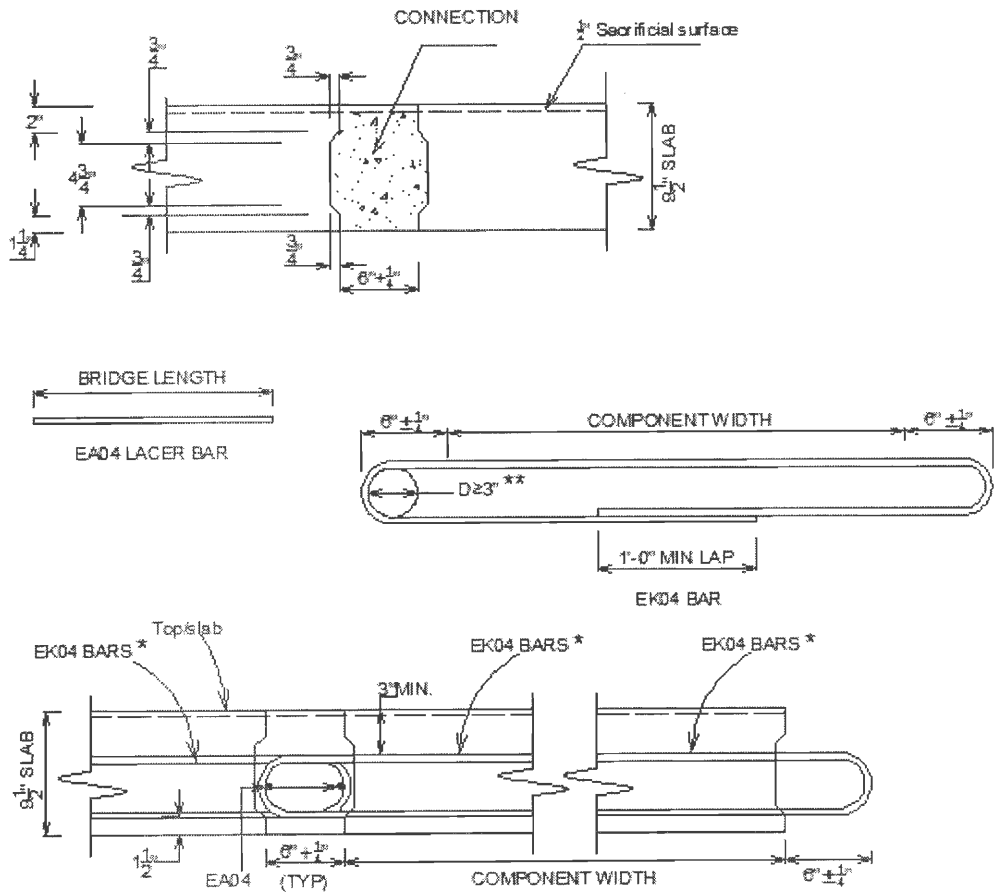

NOTES:

HIGH PERFORMANCE CONCRETE COMPRESSIVE STRENGTH IS NOT LESS THAN 7 KSI

YIELD STRENGTH OF THE STEEL IS 60 KSI

TEMPERATURE GRADIENT ZONE 3 AND HL-93 MOD LOADS WERE CONSIDERED.

* EK04 BAR SPACING IS : 11" FOR DECKED BOX-BEAM.
7" FOR OTHER DECKED PRECAST PRESTRESSED CONCRETE GIRDERS.

** DIAMETER OF BEND (D) SHALL NOT BE LESS THAN 3 IN.

Figure 44. Standardized Connection Detail Plans

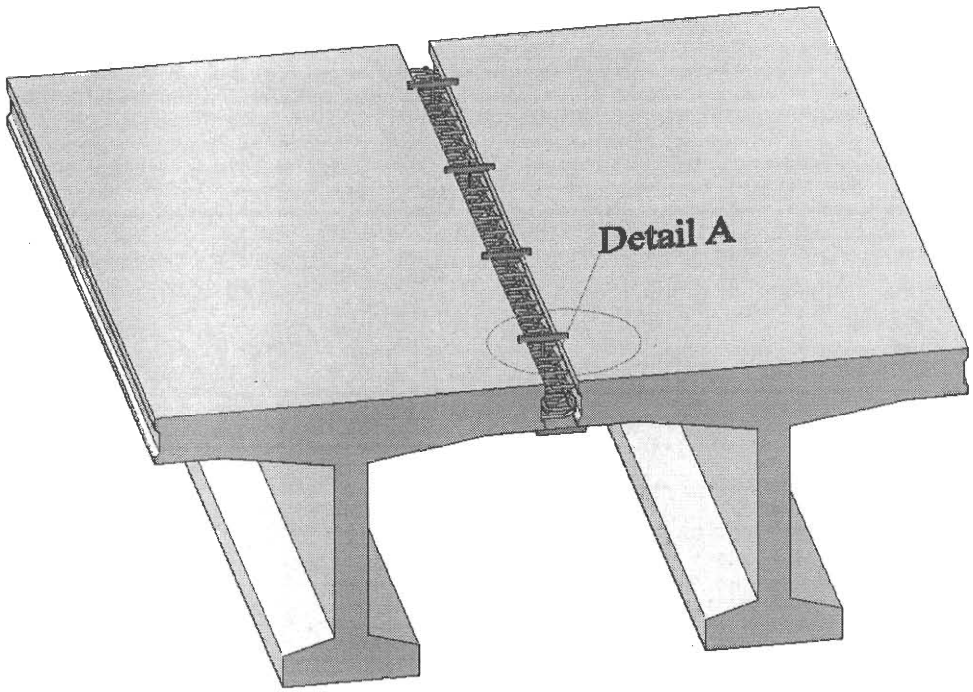

(a) Perspective View

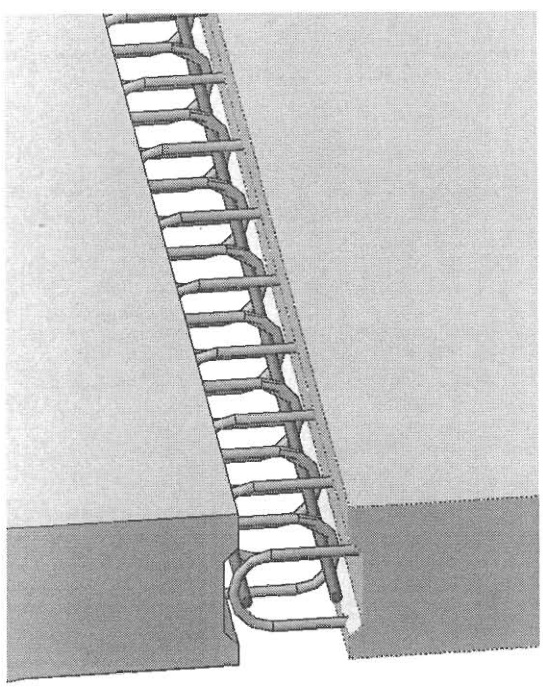

(b) Detail A

Figure 45. Standardized Connection Detail 3D View

CHAPTER 7

SUMMARY AND CONCLUSION

Prefabricated bridge elements and systems (PBES) are widely used in accelerated bridge construction (ABC). Decked precast prestressed concrete girders (DPPCG) are popular among PBES. DPPCGs are assembled and connected on site using cast-in-place grout or concrete. Even though DPPCGs offer many benefits, their use is still limited. The durability performance of connections between DPPCGs is a concern because these are the only field cast components. Neither standard design detail nor guides are available. Thus, in order to ensure a durable performance, the development of standardized connection detail is a priority. This study focused specifically on longitudinal connection between DPPCGs.

An extensive parametric study evaluated the effects of both bridge component geometry and materials on longitudinal connection load demand under various load types and magnitudes. A standardization process was presented for developing longitudinal connection detail for decked bulb-tee (DBT) and decked box-beam (DBB). Even though the example used DBT sections, the demonstrated process is equally applicable for developing a standardized detail for connections between other components. However, results of this study lead to the following conclusions:

- Temperature gradient (TG) develops moments at connections that are comparable to those of live loads (LL), and needs to be considered in the development of durable design detail.
- Sections with thicker flanges develop larger moments than those with thin flanges under TG.
- Diaphragm size has a noticeable impact on connection load demand.
- The use of materials with a high strength and a high coefficient of thermal expansion leads to greater moments at connections.

- When sections are used with thick flanges and deep concrete covers over the top reinforcement, both reinforcement layers (top and bottom) are effective in resisting positive moment.
- Control of cracking by distribution of reinforcement must be performed and the reinforcement spacing needs to be adjusted.
- Tensile stress in steel reinforcement at service limit state in AASHTO (2012) eq. 5.7.3.4-1 should have an upper limit to prevent steel reinforcement from yielding.

The ultimate product of this research was a standardized connection detail that satisfies the demand of the static and TG loads that act simultaneously on a bridge. An improved durability performance and strength equal to that of the rest of the prefabricated modules of the bridge are expected from the standardized connection detail. However, steel reinforcement spacing that is provided in the standardized connection detail is limited for the two DPPCG types (i.e., DBT and DBB). Several recommendations are addressed in order to develop standardized connection detail for other types of DPPCG types. They are:

- Connection load demand due to LL and TG for each type of DPPCG is different resulting in different connection reinforcement. Therefore, each DPPCG type needs to be investigated separately.
- TG profiles differ from region to another, thus site-specific TG profiles are required in order to perform an accurate TG analysis.
- In the structural design of the connection, the weak bond strength at the interface was not considered. It is necessary to identify material or an application procedure to enhance interface bond strength such that the connection strength is either similar to or greater than the prefabricated element strength.
- Experimental testing should be performed in future studies to evaluate the performance of the standardized connection.

REFERENCES

AASHTO (2012). ASSHTO LRFD Bridge Design Specifications, Fifth Edition, Washington, DC, 2010.

Aktan, H., Ahlborn, T. M., Attanayake, U., Deshpande, Y., & Evren, U. 2009. *Condition Assessment & Methods of Abatement of Prestressed Concrete Box-Beam Deterioration – Phase II*, MDOT RC-1527, Report to the Michigan Department of Transportation, Detroit, MI.

Attanayake, U., Abudayyeh, O., Cooper, J., Mohammed, A., and Aktan, H. (2012). "The First Full-Depth Deck Panel Accelerated Bridge Construction Project in Michigan: Constructability Challenges and Lessons Learned". *J. Perform. Constr. Facil.*, ASCE, in pub.

Azizinamini, A., Power, H., E., Myers, F., G., Ozyildirim, C., H. (2013). *Bridges for Service Life beyond 100 Years: Innovative Systems, Subsystems, and Components*. Transportation Research Board of the National Academics, No SHRP2 R19A (Publication draft), Washington D.C.

Barr, J., P., Halling, W., M., Huffaker, C., and Boyle, H. (2013). " Behavior and Analysis of Integral Abutment Bridge". Utah State University, Logan, UT.

Branco, A., F., and Mendes, A., P. (1993). "Thermal Actions for Concrete Bridge Design". *J. of Struc. Eng.*, ASCE 119(8)

Burdet, L., O. (2010). "Thermal Effects in the Long-Term Monitoring of Bridges". Large Structures and Infrastructures for Environmentally Constrained and Urbanised Areas. Lausanne, Switzerland.

Culmo, M.P. (2009). *Connection Details for Prefabricated Bridge Elements and Systems*, Technical Report FHWA-IF-09-010, Federal Highway Administration (FHWA), McLean, VA.

Culmo, M.P. (2011). *Accelerated Bridge Construction - Experience in Design, Fabrication and Erection of Prefabricated Bridge Elements and Systems,* Report FHWA-HIF-12-013, Federal Highway Administration (FHWA), McLean, VA.

Dassault Systems Simulia Corp. (2012). *Abaqus 6.10, Analysis user's manual.*

DeStefano, R., J., J. Evans, M. K. Tadros, and C. Sun. (2003). "Flexural crack control in concrete bridge structures". *PCI Convention.*

DeWolf, J., Conn, P., and O'Leary, P. (1995). "Continuous monitoring of bridge structures." Proc., Int. Assoc. Bridge Struct. Eng. Symp., *International Association for Bridge and Structural Engineering, Zurich*, Switzerland, 934-940

Dragosavi'c, M., Beukel, A., V., D., and Gijsbers, F,. B., J. (1975). "Loop connections between precast concrete components loaded in bending." Heron, 20(3), 3–36.

Ductal. (2013). "Field-Cast Joint Fill Solutions for Precast Deck Panel Bridges". *Ductal JS 1000 product datasheet,* <www.ductal-lafarge.com/JS1000> (Jul. 31, 2013)

Elbadry, M., M., and Ghali, A. (1983). "Temperature variations in concrete bridges". *J. Struct. Eng,.* ASCE, 109(10), 2355-2374

French, C.E., Shield, C.K., Klaseus, D., Eriksson, W., Smith, M., Ma, Z. J., Zhu, P., Lewis, S., and Chapman, C. E. (2011). *Cast-in-Place Concrete Connections for Precast Deck Systems*. NCHRP Web-Only Document 173, Transportation Research Board of the National Academies, Washington, DC.

French, C., Shield, C., Stolarski, H., Hedegaard, B., and Jilk, B. (2009). "Instrumentation and Monitoring of I35w St. Anthony Falls Bridge".

Frosch, R. J. (2001). "Flexural crack control in reinforced concrete". *Design and construction practices to mitigate cracking, SP-204*. American Concrete Institute. Farmington Hill, MI.

Gordon, S. R.., and May, I., M. (2005). "Development of In Situ Joints for Pre-Cast Bridge Deck Units," Bridge Engineering, BEO, 1-14.

Graybeal, A., B. (2010). *Behavior of Field-Cast Ultra-High Performance Concrete Bridge Deck Connections under Cyclic and Static Structural Loading,* Report. FHWA-HRT-11-023, Federal Highway Administration, Washington, D.C.

Graybeal, A., B. (2012).*Construction of Field-Cast Ultra-High Performance Concrete Connections*, Report. FHWA-HRT-12-038. Federal Highway Administration, Washington, D.C.

Hadidi, R. and Saadeghvaziri, A. (2005). "Transverse Cracking of Concrete Bridge Decks: State-of-the-Art". *J. of Bridge Eng.,* ASCE 10(5), 503-510.

Hartwell, R., D. (2011). "Laboratory testing of Ultra High Performance Concrete deck joints for use in accelerated bridge construction". Thesis. Iowa State University, Ames, Iowa.

He, Z., Ma, J., Z., ASCE, F., Chapman, E., C., and Liu, X. (2013). "Longitudinal Joints with Accelerated Construction Features in Decked Bulb-Tee Girder Bridges: Strut-and-Tie Model and Design Guidelines". *American society of Civil Engineering.*

Hedegaard, D., B., French, E., W., C. and Shield, C., K. (2013). "Investigation of Thermal Gradient Effects in the I-35W St. Anthony Falls Bridge". *J. Bridge Eng.* ASCE, 18(9), 890-900

Jorgensen, B., H., and Hoang, C., L. (2013). "Tests and limit analysis of loop connections between precast concrete elements loaded in tension". *Engineering Structures,* Elsevier Ltd., 52, 556-569.

Kennedy, B., J., and Soliman, Hl, M. (1986). "Temperature Distribution in Concrete Bridges". *J. of Struc. Eng.* ASCE, 113(3), 475-482.

Lee J. (2012). "Investigation of Extreme Environmental Conditions and Design Thermal Gradients during Construction for Prestressed Concrete Bridge Girders". *J. of Bridge Eng.*, ASCE, 17(3), 547-556

Li, L. (2009). *Development of DBT Bridge System with Continuous Joints for Accelerated Construction.* Ph.D Dissertation. The University of Tennessee, Knoxville, TN.

Ma, Z. Ma, Z., Chaudhury, S., Millam, J., and Hulsey, J. L. (2007). "Field Test and 3D FE Modeling of Decked Bulb-Tee Bridges". *Journal of Bridge Engineering.*, ASCE, Vol. 12, No. 3.

Martin, L.D., and Osborn, A.E.N. (1983). *Connections for Modular Precast Concrete Bridge Decks*, Report No. FHWA/RD-82/106, US DOT, Federal Highway Administration.

MDOT (2013a). Bridge Design Guide. Michigan Department of Transportation, Lansing, MI.

MDOT (2013b). Bridge Design Manual. Michigan Department of Transportation, Lansing, MI.

Mosavi, A., A., Seracino, R., and Rizkalla, S. (2012). "Effect of Temperature on Daily Modal Variability of a Steel-Concrete Composite Bridge". J. of Bridge Eng., ASCE 16(2), 979-983.

Oesterle, R.G., and Elremaily, A.F. (2009). *Guidelines for Design and Construction of Decked Precast Prestressed Concrete Girder bridges*. NCHRP project No. 12-269, Final Report, National Cooperate Highway Research Program, Transportation Research Board, National Research Council, Washington, D.C. Report

PCI (2011). *Precast, Prestressed concrete Bridge Design Manual*, third edition., Precast/Prestressed Concrete Institute, Chicago, IL.

Phares, B., Rouse, J., and Miksell, J. (2013). *Laboratory and Field Testing of an Accelerated Bridge Construction Demonstration Bridge: US Highway 6 Bridge over Keg Creek,* Report. InTrans Project 11-411. Federal Highway Administration and Iowa Department of Transportation Ames, IA.

Pontis. (2010). *Michigan Bridge Inventory Database.* Michigan Department of Transportation, Lansing,

Priestley, M. J. N. (1978). "Design of concrete bridges for temperature gradients." ACI J., 75(5), 209-217.

Roberts-Wollman, C. L., Breen, J. E., and Cawrse, J. (2002). "Measurements of thermal gradients and their effects on segmental concrete bridge." *J. Bridge Eng*, ASCE 7(3), 166–174.

Rodriguez, E., L., Barr, J., P., Halling, W., M. (2013) "Temperature Effects on a Box Girder, Integral Abutment Bridge". *J. of the Perform. of Constr. Facil.* ASCE, in pub.

Russell, G. H., and Graybeal, A., B. (2013). *Ultra-High Performance Concrete: A State-of-the-Art Report for the Bridge Community*, Report. FHWA-HRT-13-060, Federal Highway Administration, Washington, D.C.

Shim, J. (2005). "Prediction of Early-Age Cracking of UHPC Materials and Structures: A Thermo-Chemo-Mechanics Approach". Master's Thesis. Massachusetts Institute of Technology, Cambridge, Ma.

SHRP2 (2012). *Innovative Bridge Designs for Rapid Renewal.* SHRP2 Project R04 Prepublication Draft, Transportation Research Board of the National Academies, Washington, D.C.

Song, Z., Xiao, J., Shen, L. (2012). "On Temperature Gradients in High-Performance Concrete Box Girder under Solar Radiation". *Advances in Structural Engineering* 15(3), 399-415

Stanton, J., and Mattock, A.H. (1986). *Load Distribution and Connection Design for Precast Stemmed Multi Beam Bridge Superstructures.* Report No. 287, National Research Council,. Transportation Research Board of the National Academies, Washington, DC.

Svirsky, A. (2013). "The National Bridge Inventory Database". *NATIONALBRIDGES.* <nationalbridges.com> (Feb. 20, 2013).

Thompson, M. K., Davis, R. T., Breen, J. E., and Kreger, M. E. (1998). *Measured behavior of a curved precast segmental concrete bridge erected by balanced cantilevering,* Report. FHWA/TX-98/1404-2, University of Texas, Austin, TX.

TXDOT (2013). *Bridge Design Manual.* Texas Department of Transportation, Austin, TX.

Appendix A

Parametric Study Results

APPENDIX A-PARAMETRIC STUDY RESULTS

1.EVALUATING DIAPHRAGM CONFIGURATION AND SPACING

Through the evaluation the model geometry and material properties were as listed in Table A-1 and A-2, respectively.

Table A-1. Model Geometry

Model	Span length (ft)	Girder size	Girder spacing (ft)	Girder flange thickness (in.)
2-DBT-girder model	100	DBT-65	6.5	6

Table A-2. Model material properties

	Material properties		
	f'_c (ksi)	E (ksi)	Thermal Coefficient(/^{0}F)
Girder	7	5072.3	6×10^{-06}
connection	5	4286.8	6×10^{-06}
Diaphragm	5	4286.8	6×10^{-06}

1.1EVALUATING THE EFFECT OF END DIAPHRAGM CONFIGURATIONS

The variable in this evaluation is the depth of the diaphragms. Full and partial depth concrete diaphragms as shown in Figure A-1 and Figure A-2 were modeled. The model geometry and material properties are listed in Table A-1 and Table A-2, respectively.

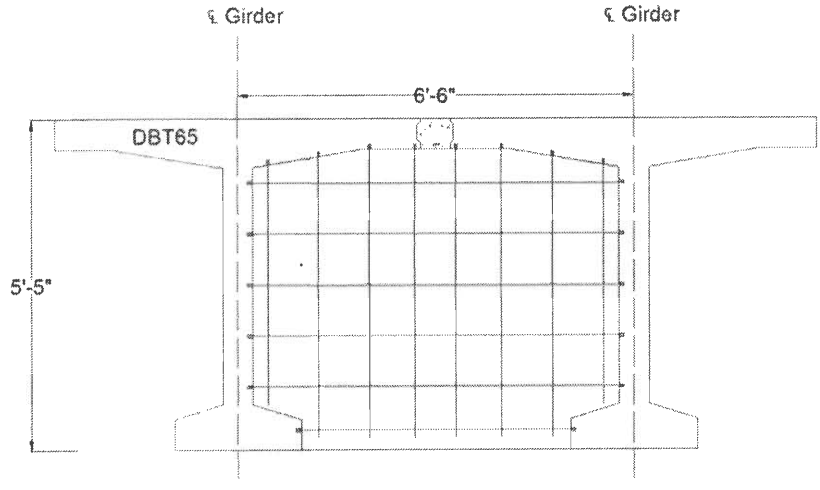

Figure A-1. End Diaphragm configuration 1

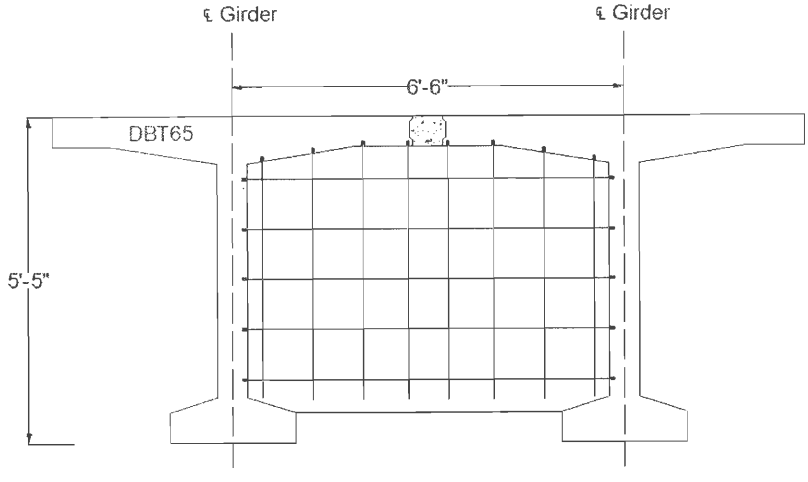

Figure A-2. End diaphragm configuration 2

Table A-3. Moment Values Developed at the Connection Due to PTG during the Evaluation of End Diaphragm Configuration Effect

	End diaphragm configuration	
	1	2
M (ft-kip/ft)	2.36	2.23

1.2EVALUATING THE EFFECT OF INTERMEDIATE DIAPHRAGM CONFIGURATIONS

Different concrete and steel intermediate diaphragm configurations (Figure A-3, Figure A-4, Figure A-5, and Figure A-6) were evaluated. All models had end diaphragm configuration 1. The number of intermediate diaphragms was 2. The model geometry and material properties are listed in Table A-1 and Table A-2, respectively.

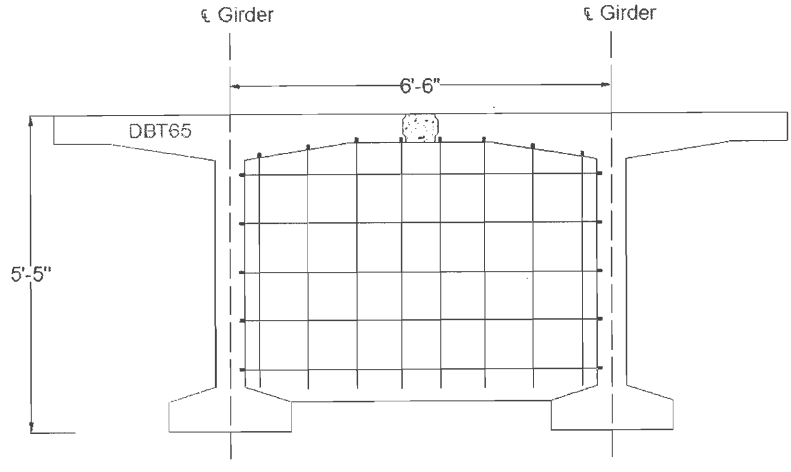

Figure A-3. Intermediate Diaphragm Configuration 1

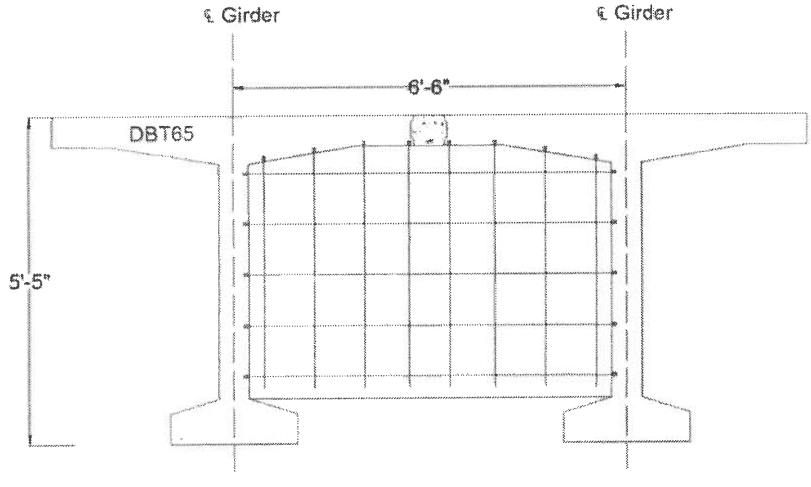

Figure A-4. Intermediate Diaphragm Configuration 2

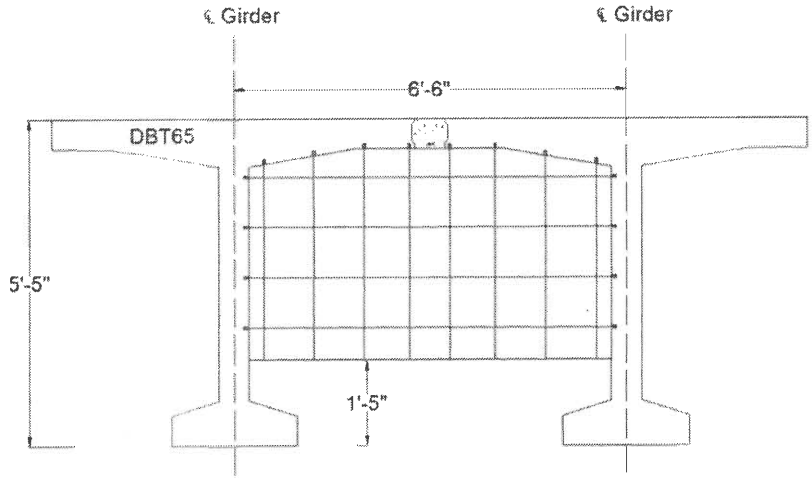

Figure A-5. Intermediate Diaphragm Configuration 3

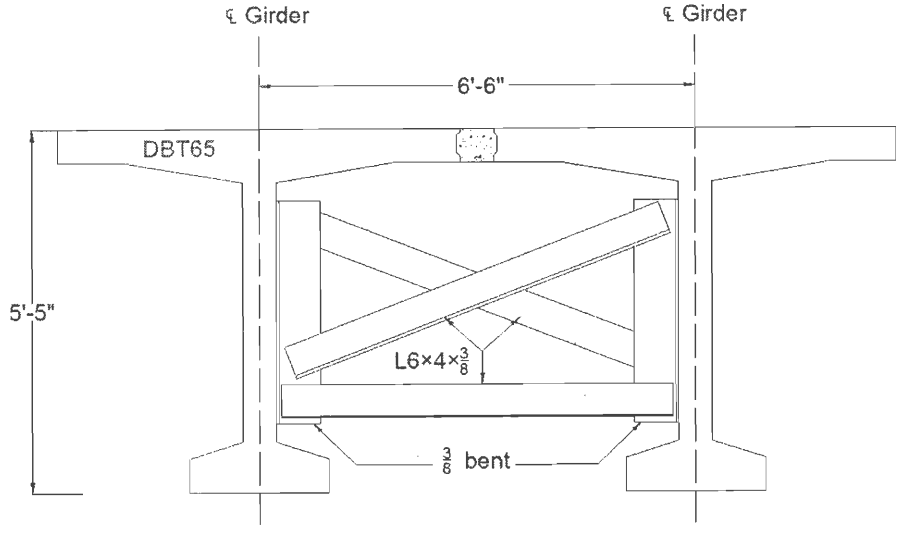

Figure A-6. Intermediate Diaphragm Configuration 4

Table A-4. Moment Values Developed at the Connection Due to PTG during the Evaluation of the Intermediate Diaphragm Configuration Effect

	Intermediate diaphragm configuration				
	No in-diaphragms	1	2	3	4
M (ft-kip/ft)	2.37	3.02	3.00	2.85	2.48

1.3EVALUATING THE EFFECT OF INTERMEDIATE DIAPHRAGM SPACING

The end and the intermediate diaphragm configurations Figure A-1 and Figure A-3 were used, respectively. The distribution of the intermediate diaphragms through the evaluation was 1 at the middle, 2 at 1/3 distances, and 3 at 1/4 distances. The model properties are given in Table A-1 and Table A-2. The obtained results are as shown in Table A-5.

Table A-5. Moment Values Developed at the Connection Due to PTG during the Evaluation of the Intermediate Diaphragm Spacing Effect

	Intermediate diaphragm spacing			
	No in-diaphragms	**1 at the middle**	**2 at each 1/3 point**	**3 at each 1/4 point**
M (ft-kip/ft)	2.37	2.62	3.02	3.15

1.4EVALUATING THE INCREASE IN BRIDGE SPAN LENGTH ACCOMPANIED WITH INCREASE IN THE NUMBER OF INTERMEDIATE DIAPHRAGM

The end and the intermediate diaphragm configurations were modeled in the evaluation are shown in Figure A-7. The bridge geometry was as given in Table A-6. Material properties were as given in Table A-7. The intermediate diaphragm spacing was as given in Table A-8.

Table A-6. Model Geometry Used in the Evaluation

Model	Span length (ft)	Girder size	Girder spacing (ft)	Girder flange thickness (in.)
Full DBB bridge	Variable	DBB-I-48	8.5	9.5

Table A-7. Model Material Properties Used in the Evaluation

	Material properties		
	f'_c (ksi)	E (ksi)	Thermal Coefficient(/^{0}F)
Girder	7	5072.3	6×10^{-06}
connection	7	5072.3	6×10^{-06}
Diaphragm	7	5072.3	6×10^{-06}

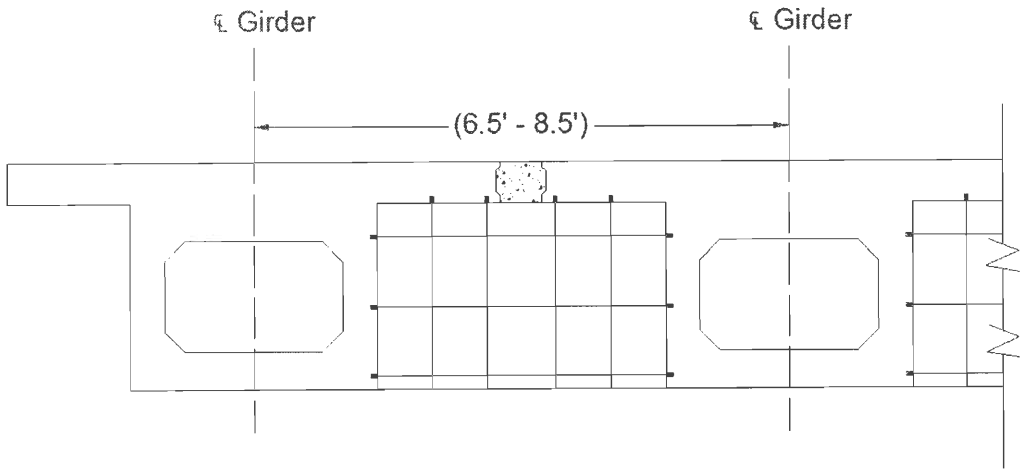

Figure A-7. End and Intermediate Diaphragm Configuration

Table A-8. DBB Intermediate Diaphragm Distribution

Span length	Location
40'	2 at center of span (11' apart)
52'	1 at center of span and 1 at each quarter point
63'	2 at center of span (11' apart) and 1 at each quarter point

2.EVALUATING THE EFFECT OF MATERIALS

Model geometry as described in Table A-1 was used in this evaluation. Models had two end and two intermediate diaphragms at 1/3 points with configurations as shown in Figure A-1 and Figure A-3, respectively. Table A-2 content was the variable in this evaluation.

2.1EVALUATING THE EFFECT OF CONNECTION MATERIAL PROPERTIES

Concrete with compressive strength of 5 ksi, and 7 ksi and thermal coefficient of $6\times10^{-06}/^{\circ}F$ was evaluated. The use of UHPC with 7200 ksi modulus of elasticity and $8.2\times10^{-06}/^{\circ}F$ coefficient of thermal expansion was included in the assessment. Girder and diaphragm materials had compressive strength of 5 ksi and coefficient of thermal expansion of $6\times10^{-06}/^{\circ}F$. The obtained results are shown in Table A-9.

Table A-9. Moment Values Developed at the Connection Due to PTG during the Evaluation of the Connection Material Effect

	Connection material properties		
	E= 4286.8 ksi, $\alpha=6\times10^{-06}/^{\circ}F$	E= 5072.3 ksi, $\alpha=6\times10^{-06}/^{\circ}F$	E= 7200 ksi, $\alpha=8.2\times10^{-06}/^{\circ}F$
M (ft-kip/ft)	2.67	2.80	3.12

2.2EVALUATING THE EFFECT OF GIRDER MATERIAL PROPERTIES

Concrete with compressive strength of 5 ksi, and 7 ksi and thermal coefficient of $6\times10^{-06}/^{\circ}F$ was evaluated. The obtained results are given in Table A-10.

Table A-10. Moment Values Developed at the Connection Due to PTG during the Evaluation of the Girder Material Effect

	Girder material properties	
	E= 4286.8 ksi, $\alpha=6\times10^{-06}/^{\circ}F$	E= 5072.3 ksi, $\alpha=6\times10^{-06}/^{\circ}F$
M (ft-kip/ft)	2.67	3.02

2.3EVALUATING THE EFFECT OF DIAPHRAGM MATERIAL PROPERTIES

Concrete with compressive strength of 5 ksi, and 7 ksi and thermal coefficient of $6\times10^{-06}/^{\circ}F$ was evaluated. The obtained results are shown in Table A-11.

Table A-11. Moment Values Developed at the Connection Due to PTG during the Evaluation of the Diaphragm Material Effect

	Diaphragm material properties	
	E= 4286.8 ksi, α=6×10^{-06}/^{0}F	E= 5072.3 ksi, α=6×10^{-06}/^{0}F
M(ft-kip/ft)	2.67	2.69

3EVALUATING THE EFFECT OF GIRDER DEPTH

Models had neither end nor intermediate diaphragms. The evaluation was performed by the full bridge model with span length of 40 ft (Table A-12). Bridge component materials were as listed in Table A-7. As shown in Table A-12. Table A-13 shows the obtained results.

Table A-12. Model Geometry Used in the Evaluation

Model	Span length (ft)	Girder size	Girder spacing (ft)	Girder flange thickness (in.)
Full DBT bridge	40	DBT-35	6.5	6

Table A-13. Moment Values Developed at the Connection Due to PTG during the Evaluation of the Girder Depth Effect

	Girder depth (in.)			
	DBT-35	DBT-41	DBT-53	DBT-65
M (ft-kip/ft)	4.58	4.67	4.77	4.83

4EVALUATING THE EFFECT OF GIRDER WIDTH

The effect of girder width was evaluated. Models had neither end nor intermediate diaphragms. Table A-7 represents material properties were considered in the analysis. Table A-6 provides model geometry. Two girder spacing were assessed (i.e., 6.5 ft and 8.5 ft). The obtained results are as shown in Table A-14. Connection moment increases when girder width increases.

Table A-14. Moment Values Developed at the Connection Due to PTG during the Evaluation of the Girder Width Effect

	Girder depth (in.)	
	DBB-I-36	DBB-I-48
M (ft-kip/ft)	8.6	9.35

5EVALUATING THE EFFECT OF GIRDER SPACING

The effect of girder spacing was evaluated. Models had neither end nor intermediate diaphragms. Respectively, Table A-12 and Table A-7 represent the model geometry and material properties were considered in the analysis. Two girder spacing were assessed (i.e., 6.5 ft and 8.5 ft). The obtained results are as shown in Table A-15.

Table A-15. Moment Values Developed at the Connection Due to PTG during the Evaluation of the Girder Spacing Effect

	Girder spacing (ft)	
	6.5	8.5
M (ft-kip/ft)	4.58	4.38

6EVALUATING THE EFFECT OF FLANGE THICKNESS

The effect of flange thickness was evaluated. Models had neither end nor intermediate diaphragms. Respectively, Table A-12 and Table A-7 represent the model geometry and material properties were considered in the analysis except that girder spacing was 8.5 ft. Two girder flange thicknesses were assessed (i.e., 6 in. and 9.5 in.). The obtained results are as shown in Table A-16.

Table A-16. Moment Values Developed at the Connection Due to PTG during the Evaluation of the Flange Thickness Effect

	Flange thickness (in.)	
	6	9.5
M (ft-kip/ft)	4.38	10.00

7 EVALUATING BRIDGE LENGTH

The effect of bridge length was evaluated. Models had neither end nor intermediate diaphragms. Respectively, Table A-12 and Table A-7 represent the model geometry and material properties were considered in the analysis. Bridges with span length of 40 ft, 80 ft, and 130 ft were modeled. The obtained results are as shown in Table A-17. The shortest span resulted in the highest moment at the connection

Table A-17. Moment Values Developed at the Connection Due to PTG during the Evaluation of Bridge Length Effect

	Bridge length (ft)		
	40	80	130
M (ft-kip/ft)	4.59	4.40	4.37

8Evaluating bridge width:

The effect of bridge width was evaluated. Models had configuration 1 end diaphragms but no intermediate diaphragms. Respectively, Table A-12 and Table A-7represent the model geometry and material properties were considered in the analysis with the exception that the girder size was DBT-41. Bridge width of 42 ft, 54 ft, and 66 ft was modeled. The obtained results are as shown in Table A-18. The bridge width has no effect on moment at the connection.

Table A-18. Moment Values Developed at the Connection Due to PTG during the Evaluation of Bridge Width Effect

	Bridge width (ft)		
	42	**54**	**66**
M (ft-kip/ft)	4.53	4.53	4.54

9EVALUATING SKEW:

The effect of skew was evaluated. Models had neither end nor intermediate diaphragms. Respectively, Table A-12 and Table A-7 represent the model geometry and material

properties were considered in the analysis. Skew of 0^0, 20^0, 30^0, and 45^0 were the scope. The obtained results are as shown in Table A-19.

Table A-19. Moment Values Developed at the Connection Due to PTG during the Evaluation of Skew Effect

	Skew ( )			
	0	20	30	45
M (ft-kip/ft)	4.58	4.5	4.38	4.35

Appendix B

Connection Design Example for DBT

APPENDIX B- CONNECTION DESIGN EXAMPLE FOR DBT

The design example illustrates the design procedure for a longitudinal connection with U-bar detail. The forces taken into the design were determined from the final DBT bridge model Table (4) when TG and LL were applied. The design was in accordance with AASHTO (2012) and MDOT (2013a, b) specifications. Flexural reinforcement that satisfies the maximum moment will be designed and crack control criteria checked. Other checks such as development length and shear capacity of the section will be performed. The following variables were used in this example:

- Connection thickness = 9 in.
- 28-day concrete compressive strength, (f'_c) = 7 ksi,
- Elastic modulus of concrete (E_c) = 5,072 ksi
- Yield strength of reinforcement (f_y) = 60 ksi,
- Elastic modulus of reinforcement (E_s) = 29,000 ksi
- Modular number (n) = 6
- Bottom concrete cover = 1.5 in. from the centerline of the bottom layer of reinforcement
- Top clear concrete cover = 3 in.
- Proposed configuration for the longitudinal connection is shown in (figure 40)

Step 1: Load Combinations for moments

Load combinations in accordance with AASHTO (2012) table 3.4.1.-1 are utilized:

Strength I:

Positive moment M_{STI-P}: 1.75(positive LL moment) = +22.75 ft-kip/ft

Negative moment M_{STI-N}: 1.75(negative LL moment) = -3.3 ft-kip/ft

Service I:

Positive moment M_{SI-P}: The greatest of

1.0 (positive LL moment+0.5 PTG moment) =18 ft-kip/ft → M_{SI-P} =+18 ft-kip/ft

1.0 (PTG moment) =+10 ft-kip/ft

Negative moment M_{SI-N}: The greatest of

1.0 (negative LL moment+0.5 NTG moment) =3.4 ft-kip/ft → $M_{SI\text{-}N}$ =-3.4 ft-kip/ft

1.0 (NTG moment) =-3 ft-kip/ft

Step2: Design for the largest moment (i.e., positive moment)

For a rectangular section, the nominal strength is given in the following equation and the required area of reinforcement steel was determined.

$$\frac{M_u}{\emptyset} = f_y d_s A_s - \left(\frac{f_y^2}{1.7 f'_c b}\right) A_s^2$$

where

A_s= cross-sectional area reinforcement steel (in^2)

b = width of rectangular section (12 in.)

d_s =distance from extreme compression fiber to the centroid of tensile reinforcement (7.5 in.)

Therefore, A_s = 0.7 in^2/ft for $M_{STI\text{-}P}$ = 22.75 ft-kip/ft was obtained and the use of #5 bars @ 5 in. satisfies the condition. However, the distance between the neutral axis and the compressive face, c is calculated as 0.9 in. from the below equation

$$c = \frac{A_s f_y}{0.85 f'_c \beta_1 b}$$

where

$$\beta_1 = 0.85 - 0.05(f'_c - 4) \text{ for } f'_c > 4 \text{ ksi}$$

The top reinforcement is located at 3 in. below the top surface which is below the natural axis, c. The strain value in the top reinforcement, (ε_s) was calculated as 0.008 which is > the yield strain of steel (i.e., the top reinforcement yields).

$$\varepsilon_s = \left(\frac{d'_s - c}{d'_s}\right)$$

where

d'_s = the effective depth for the top layer reinforcement (3.31 in.)

Thus, the section is redesigned using both layers of the U-bar to be more economical. The area of steel reinforcement A_s is 0.99 in.^{2}/ft with an effective section depth (d) = 5.5 in. Accordingly, the use of #5 bars @ 7 in. provides more economical steel reinforcement and satisfies the maximum moment requirement.

Step3: Control of cracking by distribution of reinforcement

The spacing s of mild steel reinforcement in the layer closest to the tension face shall satisfy the maximum spacing S, given in AASHTO (2012) eq. 5.7.3.4-1 as follows:

$$S = 700\frac{\gamma_e}{\beta_s . f_{ss}} - 2d_c \; ; \; \beta_s = 1 + \frac{d_c}{0.7(h - d_c)}$$

where

γ_e=an exposure factor (i.e., 1 for class exposure 1 and 0.75 for class exposure 2)

d_c=thickness of concrete cover measured from tension fiber to center of the flexural reinforcement (in.)

f_{ss}=tensile stress in steel reinforcement at the service limit state (ksi).

h=structural component total depth (in.).

d_t=distance from the extreme compression fiber to the centroid of the extreme tension steel element (in.).

Reinforcement spacing = 7 in. when #5 bar is used. Assume the neutral axis is at a distance "y" from the compression face of the section.

Transformed steel area = (steel area) × (modular ratio) = 0.31×6 = 1.86 in^2

From the compatibility equation

Tension = compression

1.86(7.5-y) =7.y. (y/2)

y = 1.75 in.

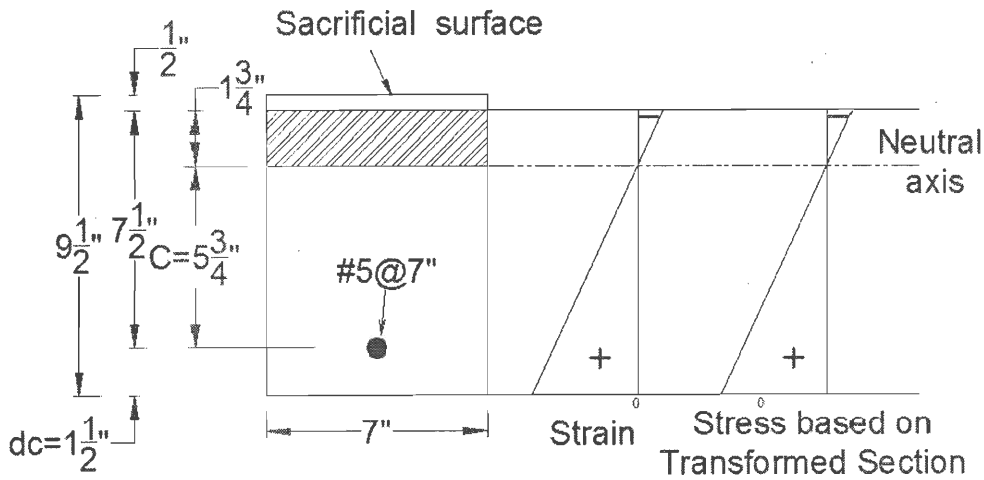

Figure B-1. Strain and Stress Diagrams.

$I_{transformed} = 1.86\times(7.5\text{-}1.75)^2 + 7\times(1.75)^3/3 = 74\ in^4$

Steel stresses, f_{ss} = (MC/I) (n) where M is the maximum positive service moment ($M_{SI\text{-}P}$) acting on 7 in. width of the connection due to live and temperature gradient loads.

$f_{ss} = [[18\times(7/12)\times(12)\times(5.75)]/74]\times 6 = 58.75$ ksi.

h= 9.5 in. - 0.5 in. = 9 in.

$$\beta_s = 1 + \frac{d_c}{0.7(h - d_c)} = 1 + \frac{1.5}{0.7(9 - 1.5)} = 1.28$$

If exposure 2 condition is assumed, $\gamma e = 0.75$. Therefore,

$$S \leq 700\frac{\gamma_e}{\beta_s \times f_{ss}} - 2d_c \quad = 700 \times \frac{0.75}{1.28 \times 58.75} - 2 \times 1.5 = 3.9 \text{ in.}$$

Since the reinforcement spacing is 7 in., which is > S, and the tensile stress in steel reinforcement f_{ss} is close to the yield stress of the reinforcement, therefore, the condition is not satisfied and crack control governs. The reinforcement was redistributed by changing the bar diameter to #4. When # 4 bar @4 in. is used, f_{ss} = 53 ksi, and S= 4.7 in. Therefore, crack control check is satisfied. Yet, the steel stress (f_{ss}) is very high, around 90% of the steel yield strength (f_y). For service limit states, this value seems unacceptable. The AASHTO (2012) eq. 5.7.3.4-1 does not have an upper limit to the tensile stresses (f_{ss}). However, the original sources for this equation Frosch (2001) and

DeStefano et al. (2003) limit f_{ss} to be 80% of steel yield strength. Hence, the detail was revised #4 @ 3.5 in.

Transformed steel area = (steel area) × (modular ratio) = 0.2×6 = 1.2 in^2

From the compatibility equation

Tension = compression

1.2(7.5-y) =3.5.y. (y/2)

y = 1.95 in.

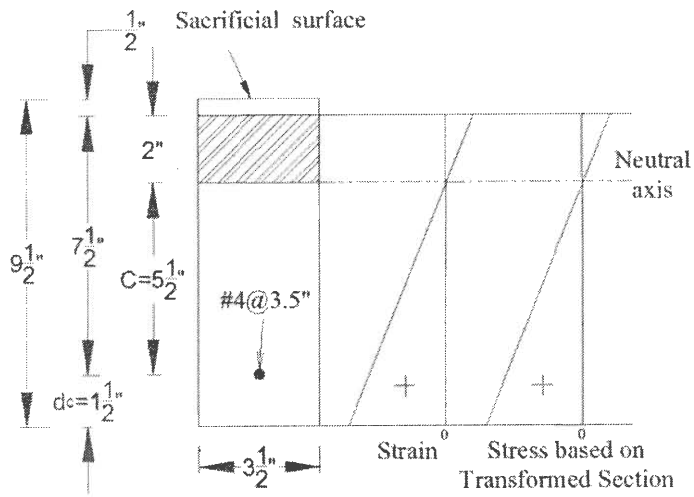

Figure B-2. Strain and Stress Diagrams

$I_{transformed} = 1.2\times(7.5\text{-}1.95)^2 + 3.5\times(1.95)^3/3 = 45\ in^4$

Steel stresses, f_{ss} = (MC/I) (n) where M is the maximum positive service moment ($M_{SI\text{-}P}$) acting on 3.5 in. width of the connection due to live and temperature gradient loads.

$f_{ss} = [[18\times(3.5/12)\times(12)\times(5.55)]/45]\times6 = 47$ ksi.

If exposure 2 condition is assumed, $\gamma e = 0.75$. Therefore,

$$S \leq 700\frac{\gamma_e}{\beta_s \times f_{ss}} - 2d_c = 700 \times \frac{0.75}{1.28 \times 47} - 2 \times 1.5 = 5.7 \text{ in.}$$

Since the reinforcement spacing is 3.5 in., which is < S, and the tensile stress in steel reinforcement f_{ss} is less than 80% of f_y, it is recommended to use #4 @ 3.5 in U-bar reinforcement for the connection. The flexural reinforcement is staggered from adjacent flanges. Accordingly, in order to accomplish the connection required reinforcement, #4@7 in. U-bars shall be distributed in each girder flange.

Step4: Cracking Moment

Cracking moment, $M_{cr} = \frac{f_r I_g}{y}$

where

f_r= modulus or rupture = $0.24\sqrt{f'_c}$ (ksi)

I_g= gross moment of inertia (in.^{4})

y= distance from the neutral axis to the extreme tension fiber (in.)

$f_r = 0.24\sqrt{7} = 0.635$ ksi

$$I_g = \frac{bh^3}{12} = \frac{12(9)^3}{12} = 729 \text{ in.}^4 \quad \text{for a } 1 \text{ ft} - \text{section}$$

$$y = \frac{h}{2} = \frac{9}{2} = 4.5 \text{ in.}$$

$$M_{cr} = \frac{0.635(729)}{4.5(12)} = 8.6 \text{ ft} - \text{kip/ft} > M_{SI-N} = 3.4 \text{ ft} - \text{kip/ft}$$

Since the cracking moment capacity is greater than the negative moment in the service limit state, the connection will not crack under the effect of LL and TG.

Step4: Shear design

Combined effect of live and temperature gradient loads was considered. Shear design is an iterative process the final arbitrary cycle is shown here

Strength I:

Shear, S_{STI-P}: 1.75 (Live load shear) = 10 kip/ft

The nominal shear resistance, V_n, shall be the smaller of:

$V_n = V_c + V_s$

$V_n = 0.25 f'c\ b_v d_v$

where:

$V_c = 0.0316\beta\sqrt{f'c}.\ b_v d_v$

V_s = shear reinforcement nominal shear resistance

d_v = effective shear depth

= d-a/2 but not less than (0.9d) or (0.72h)

From flexural design

a= 0.83 in.

h= 9 in.

d= 5.5 in.

d_v= 5.5 – (0.5) (0.83) = 5.085 in.

But not less than:

0.9 d = 0.9(5.5) = 4.95 in.

0.72h = 0.72(9) = 6.48 in.

Thus, d_v= 6.48 in.

In order to calculate the contribution of concrete to nominal shear resistance, the following steps shall be performed:

Step 4-1: Strain in Flexural Tension Reinforcement

$$\varepsilon = \left(\frac{\frac{M_u}{dv} + 0.5N_u + 0.5(V_u - V_p)\cot\theta - A_{ps}(f_{po})}{2(E_sA_s + E_pA_{ps})}\right) \leq 0.001$$

where

M_u = moment at the critical section for shear with Strength I load combination = 22.75 ft-kip/ft

V_u= shear at the critical section for shear with Strength I load combination =10 kip/ft

N_u = normal compression force acting on the location of the critical shear with Strength I load combination =zero

f_{po} =a parameter taken as modulus of elasticity of prestressing tendons = 0 ksi

V_p= component of the effective prestressing force in the direction of the applied shear =0

θ = angle of inclination of diagonal compressive stresses = 26.5 degrees (assumed)

As= 3.4 (0.2) = 0.68 in.^{2}/ft (Flexural reinforcement of a foot section of the connection at the layer closest to the tension side). Where, the number of the bars in 1 ft = 12/reinforcement spacing= 12/3.5

$$\varepsilon = \left(\frac{\frac{22.75}{6.48} + 0 + 0.5(10-0)\cot 26.5 - 0}{2(29000(0.68)+0)} = \frac{13.54}{39440}\right.$$

$$= 0.000343$$

Step4-2: Shear Stress

$$Vu = \frac{V_u - \emptyset V_p}{\emptyset b_v d_v}$$

where

Vu = shear stress in concrete

Ø = resistance factor =0.9

V_p= component of the effective prestressing force in the direction of the applied shear = 0

$V_u = \frac{10-(0.9)(0)}{(0.9)(12)(6.48)} = 0.143$ ksi

(Vu/f'c) = (0.143/7) = 0.02

Step4-3: Values of β and θ

These values were obtained from AASHTO (2012) Table 5.8.3.4.2-1

θ = 26.6° ≅ assumed value of 26.5°

β = 2.94

Therefore, the concrete contribution of resisting shear forces can be determined

$$Vc = 0.0316\beta\sqrt{f'c}\, b_v d_v$$

$$Vc = 0.0316(2.94)\sqrt{7}\,(12)(6.48) = 19.1 \text{ kip/ft}$$

Check:

$0.5\Phi(V_c + V_p) = 0.5(0.9)(19.1+0) = 8.6$ kip/ft

Since Vu = 10 kip/ft > $0.5\Phi(V_c + V_p)$= 8.6 kip/ft, concrete strength is not adequate to resist shear forces. Therefore, shear capacity from the flexural reinforcement shall be calculated to check the total section capacity.

$$V_s = \frac{Av.fy.dv.\cot\theta}{S} = \frac{2(0.2)(60)(6.48)\cot(26.5)}{3.5} = 89.1 \text{ kip/ft}$$

The total shear section capacity can be calculated as (0.9) (89.1 + 19.1) = 97.3 kip/ft, which is greater than the shear demand of 10 kip/ft. Therefore, the connection is capable of developing an adequate shear capacity.

Step5: Development length check

The basic development length for hooked U-bars shall be the greatest of

$$\frac{38.0d_b}{\sqrt{f'_c}} = \frac{38.0(0.5)}{\sqrt{7}} = 7.2 \text{ in.},$$

or

$8d_b = 8(0.5) = 4$ in.,

or

6 in.

When the modification factors are applied, the development length $=7.2\times0.7\times0.8\times1.2 = 4.83$ in. < 6.0 in. The development length condition is satisfied.

Step 6: Lacer Bar Design

To determine the appropriate size of lacer bars He et al. (2013) equation can be used as it follows:

$$\frac{A_{lbar}.f_{y,lbar}}{A_{ubar}\ f_{y,ubar}} \geq \frac{S}{4L_d}$$

where,

A_{lbar} = the area of one lacer bar

A_{ubar}= the area of one U-bar (i.e., the area of the two legs)

$f_{y,lbar}$ = yield strength of the lacer bars

$f_{y,ubar}$ = yield strength of the U bars

S= the spacing between the u bars

L_d= the development length

If the yield strength of the lacer bars is the same as for the connection reinforcement and the connection is reinforced with #4 @ 7in., lacer bar diameter should not be less than 0.385 in. Hence, it is recommended to use #4 lacer bars for the connection.

Appendix C

Connection Design Example for DBB

APPENDIX C-CONNECTION DESIGN EXAMPLE FOR DBB

The design example illustrates the design procedure for a longitudinal connection with U-bar detail. The forces taken into the design were determined from the final DBB bridge model Table (4) when TG and LL were applied. The design was in accordance with AASHTO (2012) and MDOT (2013a, b) specifications. Flexural reinforcement that satisfies the maximum moment will be designed and crack control criteria checked. Other checks such as development length and shear capacity of the section will be performed. The following variables were used in this example:

- Connection thickness = 9 in.
- 28-day concrete compressive strength, (f'_c) = 7 ksi,
- Elastic modulus of concrete (E_c) = 5,072 ksi
- Yield strength of reinforcement (f_y) = 60 ksi,
- Elastic modulus of reinforcement (E_s) = 29,000 ksi
- Modular number (n) = 6
- Bottom concrete cover = 1.5 in. from the centerline of the bottom layer of reinforcement
- Top clear concrete cover = 3 in.
- Proposed configuration for the longitudinal connection is shown in (figure 40)

Step 1: Load Combinations for Moments

Load combinations in accordance with AASHTO (2012) table 3.4.1.-1 are utilized:

Strength I:

Positive moment M_{STI-P}: 1.75(positive LL moment) = +10.5 ft-kip/ft

Negative moment M_{STI-N}: 1.75(negative LL moment) = -1.0 ft-kip/ft

Service I:

Positive moment M_{SI-P}: The greatest of

1.0 (positive LL moment+0.5 PTG moment) =+10.7 ft-kip/ft → M_{SI-P} =+10.7 ft-kip/ft

1.0 (PTG moment) =+9.3 ft-kip/ft

Negative moment $M_{SI\text{-}N}$: The greatest of

1.0 (negative LL moment+0.5 NTG moment) =-2.0 ft-kip/ft

1.0 (NTG moment) =-2.8 ft-kip/ft → $M_{SI\text{-}N}$ =-2.8 ft-kip/ft

Step2: Design for the Largest Moment (i.e., Positive Moment)

For a rectangular section, the nominal strength is given in the following equation and the required area of reinforcement steel was determined.

$$\frac{M_u}{\emptyset} = f_y d_s A_s - \left(\frac{f_y^2}{1.7 f'_c b}\right) A_s^2$$

where:

A_s= cross-sectional area reinforcement steel (in^2)

b = width of rectangular section (12 in.)

d_s =distance from extreme compression fiber to the centroid of tensile reinforcement (7.5 in.)

Therefore, A_s = 0.32 in^2/ft for $M_{STI\text{-}P}$ = 10.5 ft-kip/ft was obtained and the use of #5 bars @ 11 in. satisfies the condition. However, the distance between the neutral axis and the compressive face, c is calculated as 0.4 in. from the below equation

$$c = \frac{A_s f_y}{0.85 f'_c \beta_1 b}$$

where:

$$\beta_1 = 0.85 - 0.05(f'_c - 4) \text{ for } f'_c > 4 \text{ ksi}$$

The top reinforcement is located at 3 in. below the top surface which is below the natural axis, c. The strain value in the top reinforcement, (ε_s) was calculated the equation below as 0.02 which is greater than the yield strain of steel (i.e., the top reinforcement yields).

$$\varepsilon_s = \left(\frac{d'_s - c}{d'_s}\right)$$

where

d'_s = the effective depth for the top layer reinforcement (3.31 in.)

Thus, the section is redesigned using both layers of the U-bar to be more economical. The area of steel reinforcement A_s is 0.44 in.^{2}/ft with an effective section depth (d) = 5.5 in. Accordingly, the use of #4 bars @ 10 in. provides more economical steel reinforcement and satisfies the maximum moment requirement.

Step3: Control of Cracking by Distribution of Reinforcement

The spacing s of mild steel reinforcement in the layer closest to the tension face shall satisfy the maximum spacing S, where:

$$S = 700\frac{\gamma_e}{\beta_s.f_{ss}} - 2d_c \; ; \; \beta_s = 1 + \frac{d_c}{0.7(h - d_c)}$$

where,

γ_e = an exposure factor (i.e., 1 for class exposure 1 and 0.75 for class exposure 2)

d_c = thickness of concrete cover measured from tension fiber to center of the flexural reinforcement (in.)

f_{ss} = tensile stress in steel reinforcement at the service limit state (ksi).

h = structural component total depth (in.).

d_t = distance from the extreme compression fiber to the centroid of the extreme tension steel element (in.).

Reinforcement spacing = 10 in. when #4 bars are used. Assume the neutral axis is at a distance "y" from the compression face of the section.

Transformed steel area = (steel area) × (modular ratio) = 0.2×6 = 1.2 in^2

From the compatibility equation

Tension = compression

1.2(7.5-y) =10.y. (y/2)

y = 1.22 in.

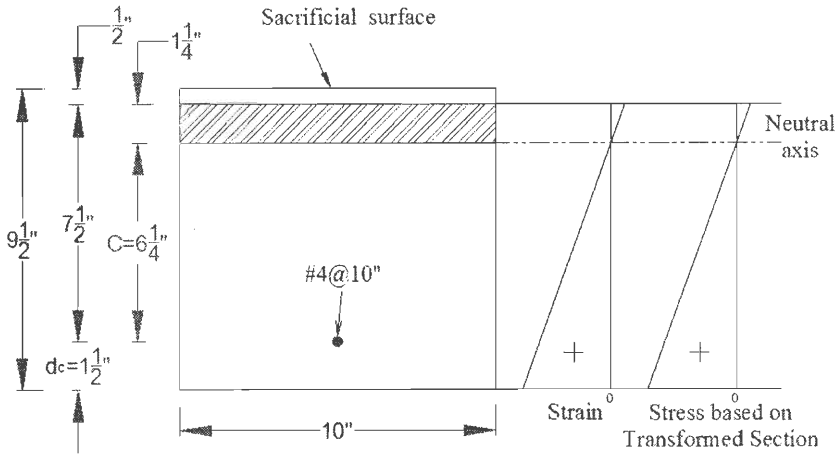

Figure C-1. Strain and Stress Diagrams.

$I_{transformed} = 1.2\times(7.5\text{-}1.22)^2 + 10\times(1.22)^3/3 = 53\ in^4$

Steel stresses, f_{ss} = (MC/I) (n) where M is the maximum positive service moment ($M_{SI\text{-}P}$) acting on 10 in. width of the connection due to live and temperature gradient loads.

$f_{ss} = [[10.7\times(10/12)\times (12)\times(6.28)]/53]\times 6 = 77$ ksi.

h= 9.5 in. - 0.5 in. = 9 in.

$$\beta_s = 1 + \frac{d_c}{0.7(h - d_c)} = 1 + \frac{1.5}{0.7(9 - 1.5)} = 1.28$$

If exposure 2 condition is assumed, $\gamma e = 0.75$. Therefore,

$$S \leq 700\frac{\gamma_e}{\beta_s \times f_{ss}} - 2d_c \quad = 700 \times \frac{0.75}{1.28 \times 77} - 2 \times 1.5 = 2.3\ \text{in.}$$

Since the reinforcement spacing is 10 in., which is > S, and the tensile stress in steel reinforcement f_{ss} is higher than the yield stress of the reinforcement, therefore, the condition is not satisfied and crack control governs. The reinforcement spacing is decreased to satisfy crack criteria. If #4@5.5in. is used, f_{ss} = 43 ksi, and S= 6.5 in. Therefore, crack control check is satisfied. The flexural reinforcement is staggered from adjacent flanges. Accordingly, in order to accomplish the connection required reinforcement, #4@11 in. U-bars shall be distributed in each girder flange.

Step4: Cracking Moment

Cracking moment, $M_{cr} = \frac{f_r I_g}{y}$

where:

f_r =modulus or rupture = $0.24\sqrt{f'_c}$ (ksi)

I_g= gross moment of inertia (in.^{4})

y= distance from the neutral axis to the extreme tension fiber (in.)

$f_r = 0.24\sqrt{7} = 0.635$ ksi

$$I_g = \frac{bh^3}{12} = \frac{12(9)^3}{12} = 729 \text{ in.}^4 \quad \text{for a 1 ft} - \text{section}$$

$$y = \frac{h}{2} = \frac{9}{2} = 4.5 \text{ in.}$$

$$M_{cr} = \frac{0.635(729)}{4.5(12)} = 8.6 \text{ ft} - \text{kip/ft} > M_{SI-N} = 2.8 \text{ ft} - \text{kip/ft}$$

Since the cracking moment capacity is greater than the negative moment in the service limit state, the connection will not crack under the effect of LL and TG.

Step4: Shear Design

Combined effect of live and temperature gradient loads was considered. Shear design is an iterative process the final arbitrary cycle is shown here

Strength I:

Shear, S_{STI-P}: 1.75 (Live load shear) = 9 kip/ft

The nominal shear resistance, V_n, shall be the smaller of:

$V_n = V_c + V_s$

$V_n = 0.25 f'c\ b_v d_v$

where:

$V_c = 0.0316\beta\sqrt{f'c}.\ b_v d_v$

V_s = shear reinforcement nominal shear resistance

d_v = effective shear depth

= d-a/2 but not less than (0.9d) or (0.72h)

From flexural design

a= 0.83 in.

h= 9 in.

d= 5.5 in.

d_v= 5.5 – (0.5) (0.83) = 5.085 in.

But not less than:

0.9 d = 0.9(5.5) = 4.95 in.

0.72h = 0.72(9) = 6.48 in.

Thus, d_v= 6.48 in.

In order to calculate the contribution of concrete to nominal shear resistance, the following steps shall be performed:

Step 4-1: Strain in Flexural Tension Reinforcement

$$\varepsilon = \left(\frac{\frac{M_u}{dv} + 0.5N_u + 0.5(V_u - V_p)\cot\theta - A_{ps}(f_{po})}{2(E_s A_s + E_p A_{ps})} \right) \leq 0.001$$

where

M_u = moment at the critical section for shear with Strength I load combination = 10.5 ft-kip/ft

V_u= shear at the critical section for shear with Strength I load combination =9 kip/ft

N_u = normal compression force acting on the location of the critical shear with Strength I load combination =zero

f_{po} =a parameter taken as modulus of elasticity of prestressing tendons = 0 ksi

V_p= component of the effective prestressing force in the direction of the applied shear =0

θ = angle of inclination of diagonal compressive stresses = 26.5 degrees (assumed)

As= 2.2 (0.2) = 0.44 in.^{2}/ft (Flexural reinforcement of a foot section of the connection at the layer closest to the tension side). Where, the number of the bars in 1 ft = 12/reinforcement spacing= 12/5.5=2.2

$$\varepsilon = \left(\frac{\frac{10.5}{6.48} + 0 + 0.5(9-0)\cot 26.5 - 0}{2(29000(0.44)+0)} \right) = \frac{10.6}{25520}$$

$$= 0.000415$$

Step4-2: Shear Stress

$$Vu = \frac{V_u - \emptyset V_p}{\emptyset b_v d_v}$$

where

Vu = shear stress in concrete

Ø = resistance factor =0.9

V_p= component of the effective prestressing force in the direction of the applied shear = 0

$$V_u = \frac{10-(0.9)(0)}{(0.9)(12)(6.48)} = 0.143 \text{ ksi}$$

(Vu/f'c) = (0.143/7) = 0.02

Step4-3: Values of β and θ

These values were obtained from AASHTO (2012) Table 5.8.3.4.2-1

θ = 26.6° ≅ assumed value of 26.5°

β = 2.94

Therefore, the concrete contribution of resisting shear forces can be determined

$$Vc = 0.0316\beta\sqrt{f'c}\, b_v d_v$$

$$Vc = 0.0316(2.94)\sqrt{7}\,(12)(6.48) = 19.1 \text{ kip/ft}$$

Check:

$0.5\Phi(V_c + V_p) = 0.5(0.9)(19.1+0) = 8.6$ kip/ft

Since Vu = 9 kip/ft > $0.5\Phi(V_c + V_p)$= 8.6 kip/ft, concrete strength is not adequate to resist shear forces. Therefore, shear capacity from the flexural reinforcement shall be calculated to check the total section capacity.

$$V_s = \frac{Av.fy.dv.\cot\theta}{S} = \frac{2(0.2)(60)(6.48)\cot(26.5)}{5.5} = 56.7 \text{ kip/ft}$$

The total shear section capacity can be calculated as (0.9) (56.7 + 19.1) = 68.2 kip/ft, which is greater than the shear demand of 9 kip/ft. Therefore, the connection is capable of developing an adequate shear capacity.

Step5: Development Length Check

The basic development length for hooked U-bars shall be the greatest of

$$\frac{38.0d_b}{\sqrt{f'_c}} = \frac{38.0(0.5)}{\sqrt{7}} = 7.2 \text{ in.},$$

or

$8d_b = 8(0.5) = 4$ in.,

or

6 in.

When the modification factors are applied, the development length =7.2×0.7×0.8×1.2 = 4.83 in. < 6.0 in. The development length condition is satisfied.

Step 6: Lacer Bar Design

To determine the appropriate size of lacer bars He et al. (2013) equation can be used as it follows:

$$\frac{A_{lbar}.f_{y,lbar}}{A_{ubar}\, f_{y,ubar}} \geq \frac{S}{4L_d}$$

where,

A_{lbar} = the area of one lacer bar

A_{ubar}= the area of one U-bar (i.e., the area of the two legs)

$f_{y,lbar}$ = yield strength of the lacer bars

$f_{y,ubar}$ = yield strength of the U bars

S= the spacing between the u bars

L_d= the development length

If the yield strength of the lacer bars is the same as for the connection reinforcement and the connection is reinforced with #4 @ 11in., lacer bar diameter should not be less than 0.483 in. Hence, it is recommended to use #4 lacer bars for the connection.